The Evolutionary Consequences of Stars Near the Eddington Limit

Author:
Durand D'souza

Supervisor:
Prof. Norbert Langer

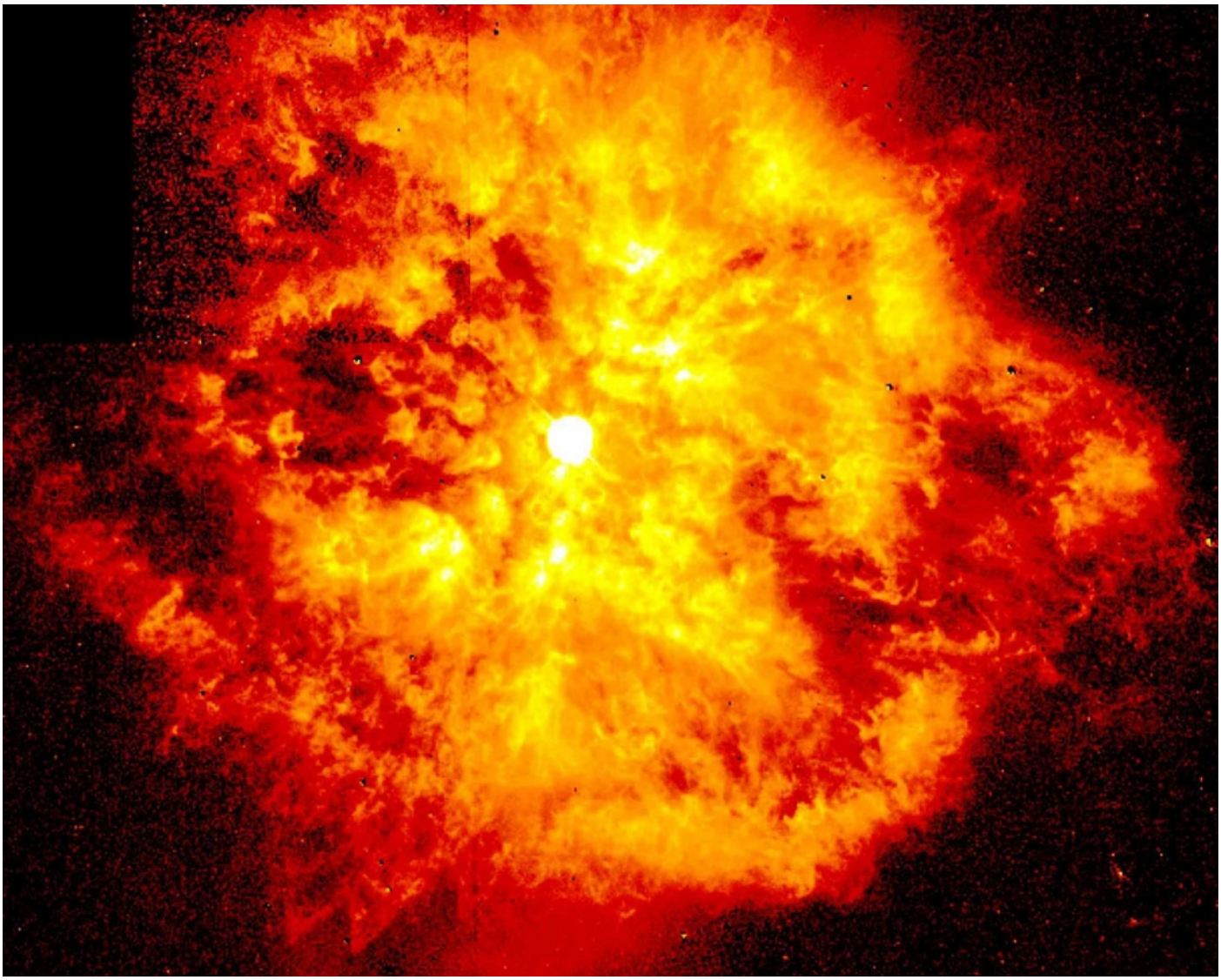

Stellar Physics group
Argelander Institut für Astronomie
2012

Acknowledgments

First and foremost I would like to thank my supervisor, Prof. Norbert Langer, for allowing me to work in the Stellar Physics group, for the long hours he put into my project guiding me through the investigation, the helpful discussions we had and for all the constructive criticism. I wouldn't be writing this if it weren't for you. I would also like to acknowledge Karen K'ohler for getting me set up with the Binary Evolution Code and debugging its problems, pointing out relevant literature and helping me understand numerous other bits of knowledge. Dr. Hilding Neilson was also instrumental in getting me to this point by answering all the silly questions I had. I thank Dr. Sung-Chul Yoon for explaining to me the structure of BEC and for pointing out problems when it didn't work and Dr. Johannes Knapp for arranging this extended project and helping me with the application process so that I could spend five months in such a fantastic group. Finally, I thank all my colleagues in the Stellar Physics group and outside it for making this amazing experience a hundred times better!

Unless otherwise acknowledged, the following report contains my own unaided work. - Durand D'souza (25/06/12)

Cover page image: NASA Hubble Space Telescope picture of the energetic star WR124

Credit: Yves Grosdidier (University of Montreal and Observatoire de Strasbourg), Anthony Moffat (Universitie de Montreal), Gilles Joncas (Universite Laval), Agnes Acker (Observatoire de Strasbourg), and NASA

The Evolutionary Consequences of Stars Near the Eddington Limit

Durand D'souza

Department of Physics and Astronomy, University of Leeds, Leeds, UK, 2012

ABSTRACT

We developed a new theoretical mass loss prescription for luminous stars near the Eddington Limit. Using a 1D hydrodynamic stellar structure and evolution code, we qualitatively considered the implications of this Eddington mass loss on the evolution of masive stars between 60 and 100 solar masses as well as the effects of rotational mass loss and angular momentum loss by calculating stars initially rotating up to 350 km/s. Our mass loss prescription varies the mass loss rate as a function of the maximum Eddington factor in the star and its optical depth and we identified its effectiveness in explaining the Humphreys-Davidson limit.
We found that our mass loss prescription was quite successful in modelling the Humphreys-Davidson limit, albeit at a slightly cooler effective temperature. We also found that changing the free parameters of our prescription lead to non-linear effects that, with sufficient calibration from observations, may produce accurate results for high mass stars greater than $60M_{\odot}$. However, we were unable to reproduce the same effect with $60M_{\odot}$ stars that were not rotating quickly and modifying the free parameters were found to only be marginally effective for these models. We question the accuracy of the large mass loss rates applied to models very close to the Eddington limit as these are slightly larger than observations. We conclude by recommending this mass loss prescription for use in evolutionary calculations but only after it has been calibrated further.

Table of Contents

List of Figures

Chapter 1

Introduction

On a clear night, one may see several million stars with a quick glance. These stars are not all alike. Some are sun-like stars which live for billions of years and die quietly. Others may interact with their binary companions and produce exotic new objects. More massive stars shine a million times as brightly as our Sun but only live for a fraction of the time. All these stars will contribute to the evolution of the Universe through chemistry, dynamics and the impact on their local environment. There are thought to be 10^{12} stars in our galaxy alone and a clear understanding of all of them is needed to know our place in the Universe.

1.1 Hydrostatic Equilibrium

Stars are in hydrostatic equilibrium for most of their lives. This is where the outward force of internal pressure is balanced by the inward pull of gravity. Other phenomena - rotation, magnetism, binarity - may also influence this equilibrium. In this section, we consider a basic model of a star with only forces due to internal pressure and gravity.

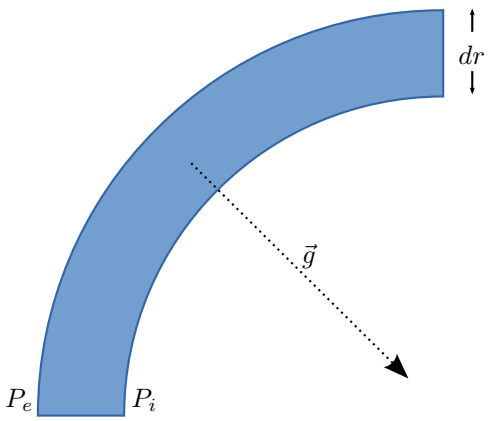

Fig. 1.1: A difference in pressure $P_i - P_e$ creates a force that must be balanced by gravity for a star to remain in hydrostatic equilibrium.

We use Kippenhahn & Weigert (1994), hereafter Kippenhahn and Weigert, for this derivation. For a given snapshot in time, consider a thin spherical mass shell with infinitesimal thickness dr at a radius r in the star. The mass of the shell per unit area is ρdr so the gravitational force acting on it is $-g\rho dr$. For a hydrostatic situation, the gravitational force must be balanced by the force due to pressure. This means that the pressure must be larger at the interior of the shell than the exterior. The force, per unit area, acting on the shell due to the pressure is

$$P_i - P_e = -\frac{\partial P}{\partial r} dr \tag{1.1}$$

The sum of the forces must be zero so

$$\frac{\partial P}{\partial r} + g\rho = 0 \tag{1.2}$$

which is the equation of Hydrostatic Equilibrium. In Lagrangian mass coordinates (where $\frac{\partial r}{\partial m} = \frac{1}{4\pi r^2 \rho}$) and after substituting in Newton's Law of Gravitation, it becomes

$$\frac{dP}{dm} = -\frac{Gm}{4\pi r^4} \tag{1.3}$$

If the two terms don't balance, the star is in a hydrodynamic situation and a much more vigorous treatment must be used to describe the stellar interior.

1.2 Star formation

Star formation begins with a giant molecular cloud of tens of thousands of solar masses which becomes unstable to collapse when its mass becomes larger than the Jeans Mass. This change could be triggered by several factors including collisions with other clouds, shock waves from supernovae and ionisation from hot stars (Prialnik 2000). The cloud may fragment if the mass of the fragment is larger than its Jeans Mass. The mass of these fragments determine the final mass of the star as well and the fragmentation process determines the IMF of the cloud. As it contracts, its gravitational energy decreases and it partially radiates this away. At some point, the fragment reaches a critical temperature and deuterium fusion begins and a protostar is born. The radiation pressure from this slows down collapse but does not halt it and matter continues to accrete onto the protostar. Eventually, the core temperature and density is high enough for hydrogen fusion to ignite. Radiation pressure from this then blows away any matter around the star, which is now officially on the main sequence. Its structure is defined by its mass, metallicity and rotational velocity.

1.3 Energy transport in stars

Energy generated inside the star must be transported through the stellar interior to get to the surface. Depending on the local conditions, this may occur via three processes:

- Conduction
- Radiation
- Convection

1.3.1 Conduction

Energy is transferred via conduction when particles, which could be ions or elections, collide with each other. In a non-degenerate gas, the cross section of collisions between these particles is very small ($10^{-18} - 10^{-20} cm^2$ per particle

(Kippenhahn and Weigert)) owing to the high density and temperature. In later stages of evolution, the core may become degenerate and conduction becomes an important method of energy transport but this stage will not be covered here.

1.3.2 Radiation

The transfer of energy via photons is known as radiation. Stellar matter is very opaque and photons will, for example, have a mean free path of $l_{ph} \approx 2cm$ (Kippenhahn and Weigert) in the sun. Because of the small mean free path of the photons relative the the stellar radius R, energy transport via radiation may be treated as a diffusion process. The basic equation for radiative transport of energy is

$$\frac{dT}{dm} = -\frac{3}{64\pi^2 ac}\frac{\kappa_{rad} l}{r^4 T^3}. \tag{1.4}$$

The assumption of a small mean free path becomes invalid as we approach the surface of the star so this equation does not hold and instead a full treatment of radiation in the stellar atmosphere is required. κ_{rad} is the mean opacity at each point, which considers the effect of photons of different frequencies (with different mean free paths) travelling through the medium as well as the different opacities of different gases - elections, hydrogen, helium and heavier ions and when approaching the surface of low mass stars, molecules and dust particles - constitute the medium. A effect particularly important for this work is the treatment of opacity peaks of ions. At a particular temperature, the spin-orbit interaction of an atom becomes significant and a peak in the opacity is produced (Iglesias et al. 1992). The strongest peak comes from Fe at $log(T[K]) = 5.25$, followed by a weaker peak for He at $log(T[K]) = 4.70$ and even weaker, H. The prominence of the Fe peak increases with metallicity (Cantiello et al. 2009; Iglesias et al. 1992).

A dimensionless radiative temperature gradient, ∇_{rad}, may be found by combining (1.4) with (1.3)

$$\frac{dT}{dm} = \frac{dP}{dm}\frac{dT}{dP} = -\frac{Gm}{4\pi r^4}\frac{T}{P}.\frac{dlogT}{dlogP}, \tag{1.5}$$

$$\nabla_{rad} = \left(\frac{dlogT}{dlogP}\right)_{rad} = \frac{3}{16\pi acG}\frac{\kappa_{rad} lP}{mT^4}. \tag{1.6}$$

A photon will transfer momentum to a particle during a collision. This creates radiation pressure and in sufficient quantities, it can render a region unstable. Substituting $P_{rad} = \frac{1}{3}aT^4$ into (1.4) and converting to spherical coordinates with $\frac{\partial r}{\partial m} = \frac{1}{4\pi r^2 \rho}$ gives:

$$\frac{dP_{rad}}{dr} = -\frac{4}{3}aT^3\frac{dT}{dr} = -\frac{\kappa\rho}{4\pi c}\frac{l}{r^2}. \tag{1.7}$$

This radiation pressure must also be balanced by gravity for the star to remain in hydrostatic equilibrium and so

$$\left|\frac{dP_{rad}}{dr}\right| < \left|\left(\frac{dP}{dr}\right)_{H.E.}\right|, \tag{1.8}$$

which gives the inequality

$$\frac{\kappa\rho}{4\pi c}\frac{l}{r^2} < \frac{Gm\rho}{r^2}. \tag{1.9}$$

We can then rearrange this to get

$$l < \frac{4\pi cGm}{\kappa} = l_{Edd}. \tag{1.10}$$

We only need to look at the luminosity carried by photons so $l = l_{rad}$. This leads to an upper limit of the local luminosity, called the *Eddington Luminosity*, above which the radiation pressure drives movement within the star and hence, an alternate transport of energy is required to carry that luminosity. This alternate transport is convection (Langer 1997) and will be discussed in the next section. Equation (1.10) is not the only condition for convection and if the others are not met, convection will not occur and the layers with super-Eddington luminosities will become hydrodynamic and accelerate outwards, eventually giving rise to strong winds.

1.3.3 Convection

Convection may be considered using the simple model of a perturbed mass element in a fluid. While we assume spherical symmetry in our equations, in reality, there may be assymetric pertubations that arise due to the thermal motion of particles in gas. If these perturbations are damped, then we do not need to worry about them. On the other hand, they may be undamped and grow to create macroscopic motions in the fluid and transport matter and energy between layers. For this reason we must consider the dynamical instability of a layer to convection.

Consider a mass element that is perturbed and moved upwards in the star. It starts at a radius r with pressure $P_\star = P_1$ and density $\rho_\star = \rho_1$ and moves to $r + \Delta r$ which is at an ambient pressure P_2 and density ρ_2. In a star, pressure generally decreases outwards so the mass element expands to $P_\star = P_2$ to be in equilibrium. However, its density decreases due to this expansion and is not necessarilly equal to the ambient density. If $\rho_\star > \rho_2$, due to Archimedes' law, the element will experience a net buoyancy force downwards and it moves back to its original radius r which quenches the perturbation. If, however, it has a density $\rho_\star < \rho_2$, it experiences an upwards force and the region is unstable to convection because the perturbations are undamped. The expansion of the element as it rises occurs over the local dynamical timescale, which is typically shorter than the timescale for heat exchange. This means that the expansion will be nearly adiabatic so we can use the adiabatic exponent $\gamma_{ad} = \left(\frac{\partial logP}{\partial log\rho}\right)_{ad}$ to mathematically describe this criteria and calculate the change in density of the bubble.

$$\frac{\delta P_e}{P_e} = \gamma_{ad}\frac{\delta\rho_\star}{\rho_\star} \tag{1.11}$$

$\delta P_\star$ is determined by the pressure gradient dP/dr in the star so $\delta P_\star = P_2 - P_1 = (dP/dr)\Delta r$. So the change in density

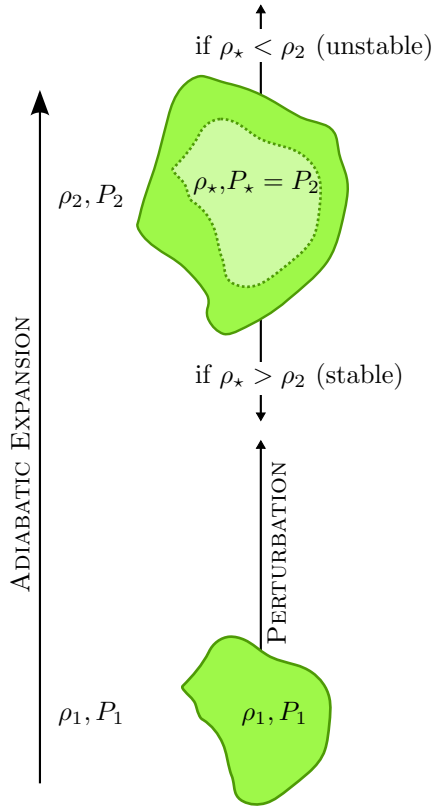

Fig. 1.2: The Schwartzschild criteria for convection: a fluid element is perturbed upwards to an environment of lower pressure and density. If expands adiabatically to equalise in pressure but it still has a different density. If this density is larger than the surroundings, it will not be buoyant and sink back down damping the perturbation. If, instead, it has a lower density, it will rise and convection sets in. Inspired by Prialnik (2000)

$\delta\rho_\star$ is then

$$\delta\rho_\star = \frac{\rho_e}{P_e}\frac{1}{\gamma_{ad}}\frac{dP}{dr}\Delta r \tag{1.12}$$

$\rho_\star = \rho_1 + \delta\rho_\star$ and $\rho_2 = \rho_1 + (dp/dr)\Delta r$, where dp/dr is the gradient in density in the star. We can then express the Schwartzschild criterion against convection $\rho_\star > \rho_2$ as

$$\delta\rho_\star > \frac{d\rho}{dr}\Delta r \tag{1.13}$$

and when we combine it with (1.12), divide by dP/dr and replace $P_\star$ and $\rho_\star$ with P and ρ we eventually get

$$\frac{dlog\rho}{dlogP} > \frac{1}{\gamma_{ad}}. \tag{1.14}$$

If a region violates this condition, convection develops. An element that is slightly hotter than its surroundings will rise until it disolves, transporting heat with it. A cooler element will move downwards and carry less heat than its surroundings. This means that when it dissolves, it will absorb heat. In general, there is a net upwards movement of heat, and luminosity making convection an efficient transport of heat. Convection is also a very efficient chemical mixing process due to the movement of mass elements and it plays a big role in massive stars which have convective cores by prolonging their main sequence lifetime as well as bringing the ashes of hydrogen burning to the surface at a faster rate.

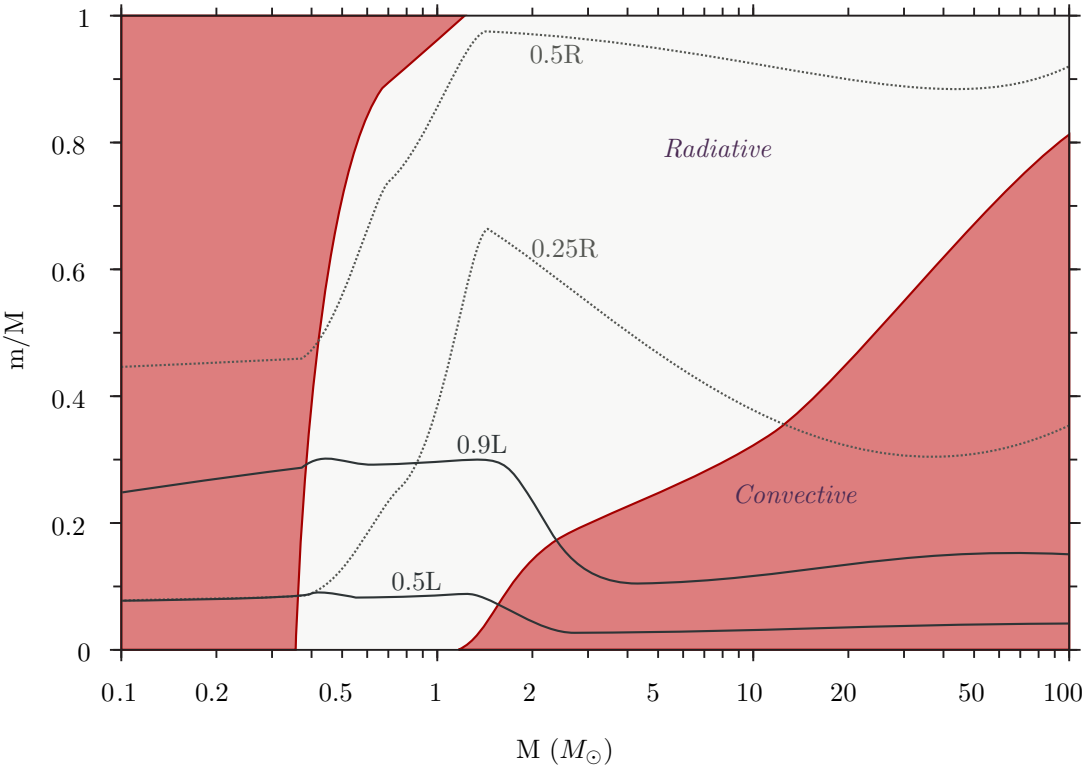

Fig. 1.3: A plot of the fractional mass of the star dominated by convection or radiation as a function of the ZAMS mass, inspired by Kippenhahn and Weigert.

1.3.4 The overall picture

Due to the varying conditions in stars of different mass, we see alternate forms of energy transport dominating.

Using the Schwartzschild criterion (1.14), we can predict the energy transport that will occur in different stars. Very low mass stars ($M < 0.35M_\odot$) are fully convective because of their high densities and low internal pressure due to weak nuclear burning. For solar mass stars ($0.35M_\odot < M < 1.3M_\odot$) the energy generation rate is higher and the weak dependence of temperature for the PP chain process means that the energy generation can spread over a larger range. The energy flux and radiative temperature gradient are then low so the core is radiative. Near the surface, the temperature is low so there are high opacities and therefore convection sets in. For high mass stars ($M > 1.3M_\odot$), the CNO cycle dominates energy generation. This has a very high temperature sensitivity so nuclear burning only occurs over a small range in the core. This means that there is a very high energy flux and radiative temperature gradient which means that convection is the only process that can carry all that luminosity out of the core. As we approach the surface, the temperature drops and there is no energy generation so the low flux and temperature gradient force the envelope to be radiative. Just below the surface, the temperatures are sufficiently low that Fe and other elements become opaque due to spin-orbit interactions. This enables convection to occur in the form of sub-surface convection zones, which are important in the study of turbulence, winds and clumping Cantiello et al. (2009).

1.4 Low mass stars

A Sun-like star with a mass $M \lesssim 1.3M_\odot$ will fuse hydrogen into helium for around 10 billion years during what is known as the Main Sequence. The temperature gradient Helium has a larger molecular weight than hydrogen. Over time, the amount of helium in the core rises and the mean molecular weight rises accordingly which leads to a proportional increase in the luminosity (as given by the relation $L \propto \mu^4$ for homogeneous stars). Helium contamination in the core decreases the rate of fusion, which in turn reduces the thermal pressure and contracts the core. This contraction increases the internal temperature and pressure (due to the ideal gas law) and hydrogen fusion occurs at a faster rate because of the temperature-energy generation relation $\epsilon_{pp} \propto T^4$ for the pp chain process governing hydrogen burning. To maintain hydrostatic equilibrium, the pressure from the outer layers of the star decreases and, as a result, the envelope expands a little. This process repeats with the core contracting and the envelope expanding over time until the star runs out of hydrogen in the core. Fusion ceases and the core subsequently contracts even further leading to a large envelope expansion due to the reduced gravitational attraction from the core. The star is now a red giant. A few million years and several further stages of evolution later, it quietly becomes a white dwarf.

1.5 Massive Stars

1.5.1 Overview

More massive stars ($M \gtrsim 1.3M_\odot$) fuse hydrogen into helium via the CNO cycle. The CNO cycle is much more sensitive to changes in the core, $\epsilon_{CNO} \propto \rho T^{18}$ so a small change in temperature can have a large effect. As the mean molecular weight in the core increases and the core contracts, increasing the central temperature, the envelope expands to maintain hydrostatic equilibrium. Due to the much higher dependence of energy generation on temperature than for stars dominated by the pp chain, this expansion is large and the star's effective temperature decreases drastically due to the Stefan-Boltzmann law. Eventually, the hydrogen in the core is exhausted, fusion subsides and the core contracts further. A hydrogen burning shell develops above the core inflating the envelope even further due to thermal pressure from the hydrogen burning shell. Eventually, the core is hot enough and dense enough for helium burning to ignite and later, exhaust itself. Carbon, Neon and Oxygen, and Silicon burning also occur subsequently on faster and faster timescales. However, for stars more massive than about $40M_\odot$, another significant process takes place which defines the later evolution - the phenomenon of dense stellar winds.

1.5.2 Winds

The solar wind is on the order of $\dot{M}_\odot = 2 \times 10^{-14}\ M_\odot/yr$ (e.g. Feldman et al. 1977). These winds are mostly driven by magnetic fields (Low 1996) and a sun-like star is not significantly affected by mass loss over the course of its main sequence life (Bloecker 1995). On the other hand, massive stars are more luminous and have radiative envelopes. These features

can drive mass loss which must be considered when modelling the evolution of these stars. Furthermore, mass loss is likely necessary to explain the Humphreys-Davidson Limit (Humphreys & Davidson 1994), a region of the Hertzsprung-Russel diagram constrained by high luminosities and cool temperatures which contains very few observed stars and is not well understood with current stellar evolution theory.

Above $10M_{\odot}$, stars begin their lives as luminous OB dwarfs. They have optically thin winds with mass loss rates of around 10^{-5} $M_{\odot}/yr$ (Lamers & Leitherer 1993) during the main sequence, several magnitudes higher than those of sun-like stars. Owing to the short lifetimes of these stars, the low frequency of massive stars in the IMF (e.g. Espinoza et al. 2009), the fact that most of them are still enshrouded in their molecular clouds and a number of other reasons mean that they are difficult to observe. Nevertheless, there have been a number of surveys of massive stars. Using the VLT-FLAMES instrument, a multi-epoch survey of massive stars in the galaxy and magellanic clouds was carried out (Evans et al. 2010) and a follow-up survey of the Tarantula nebula is in progress (Evans et al. 2011). Complementary HST observations of 30 Doradus, the region that powers the Tarantula nebula, are also planned. These future observations will narrow down the IMF of massive stars as well as provide information on the binary fraction of these stars, on their rotational velocities, winds and a number of other important details that may be used to constrain theoretical models.

1.5.3 Summary

It is vital that we understand massive stars and the mechanism behind these winds. The high temperatures of these stars give rise to large quantities of ionizing photons which reionise their environment and may even trigger star formation. Massive stars are also progenitors of supernovae which nucleosynthesise the heavy elements that are essential to life. Mass loss significantly affects the mass of the SN progenitor and may even decide the final remnant that is left behind. If the star were massive enough and did not lose much mass, it could leave behind a black hole, whereas if it did lose sufficient mass, it may not leave behind any remnant when it explodes as a pair instability supernova (see Heger & Woosley 2002, for details). Therefore, the modelling of these winds (Vink et al. 2011; Gräfener et al. 2011), their impact on the star (Maeder & Meynet 2010, 2000) and on their environment (Mackey et al. 2012; Parkin et al. 2009), is an area of active research.

1.6 Stellar Evolution code

1.6.1 Overview

Our models are calculated using a 1D hydrodynamic binary stellar evolution code (BEC) described in detail in Heger et al. (2000), with substantial updates by Petrovic et al. (2005), Yoon et al. (2006) and Brott et al. (2011). In this section, we present an overview of the physics used in the code. BEC solves the the hydrodynamic stellar structure equations (Fliegner 1993) as well as the set of nuclear abundance equations simultaneously. The star is represented

as a 1D spherically symmetric refined Lagrangian grid divided into isobaric mass shells. We use isobaric coordinates because rotation may cause the star to deviate from spherical symmetry and using isobaric shells allows us to continue assuming this symmetry. The effect of centrifugal acceleration on the stellar structure is also taken into account using the prescriptions by Kippenhahn & Thomas (1970) and Endal & Sofia (1976). The grid is refined according to local properties related to the temperature, density and mean molecular mass gradients as well as a number of other factors. In general, our models have an approximate total of 1600 grid points. We also need to consider the effects of convection, mass loss and a number of other important physical processes on the structure and evolution of the model.

1.6.2 Treatment of convection

The treatment of convection has long been a bottleneck in astrophysical problems. Coupled with our weak understanding of turbulence and the fact that simulations run over a large range of magnitudes in density, pressure, temperature and gravity make it impractical to calculate its true effects. Observational measurements to pin down various parameters related to convection have also proven difficult. Recently, however, the advances in helioseismology have made it possible to measure the depth of the Sun's convection zone to a high precision (Kosovichev 2007, e.g.) which has further highlighted the relatively inaccuracy of theoretical models. Further developments in asteroseismology have given us the tools to measure the properties of convection in other stars, as well as pin down parameters that were once unknown. In stellar evolution models, including BEC, convection is treated using the well-known Mixing Length Theory (MLT) (Biermann 1932) but only order of magnitude predictions of chemical mixing, transport, magnetic fields and other phenomena are possible (Kupka 2005). To compute convection accurately, one must solve the Navier-Stokes equation coupled with equations of stellar structure, as well as the hydrodynamic equations which, due to the non-linearity of the equations, is computationally expensive. One possible improvement was presented by Canuto & Dubovikov (1998) and later used by Kupka & Montgomery (2002) in models of A stars. New prescriptions are still too computationally expensive to run for a series of models so in this work, we stick to the Mixing Length Theory, or more specifically the Böhm-Vitense (1958) formulation of MLT. The diffusion coefficient for composition mixing is then

$$D_{conv} \equiv \alpha_{MLT} H_p \nu_{conv}/3, \tag{1.15}$$

where ν_{conv} is the convective velocity and H_p is the pressure scale height defined as

$$H_p \equiv -\frac{dr}{dlnP} = \frac{P}{\rho g}, \tag{1.16}$$

for the hydrostatic case. We use a mixing length parameter of $\alpha_{MLT} = 1.5$ (Böhm-Vitense 1958; Langer 1991). Convective overshooting, where convective material is carried into a region stable to convection due to its momentum, is also accounted for with a mass- and velocity-independent overshooting parameter of $f_{over} = 0.335$ calibrated by Brott et al. (2011) using observational properties of rotating B stars from the VLT-FLAMES survey (Hunter et al. 2008). We naïvely assume,

due to lack of information, that f_{over} applies to stars more massive than those in Hunter et al. (2008) but this may be incorrect and lead to uncertainties. The assumption of mass- and velocity-independence is also a possible uncertainty. Semiconvection is treated according to Langer et al. (1983) with an efficiency parameter of $\alpha_{sem} = 1$ (Langer 1991).

1.6.3 Treatment of Rotation

As described in 1.6.1, rotation is treated by modifying the hydrodynamic stellar structure equations to include centrifugal acceleration. The transport of angular momentum must also be considered and this is treated as a diffusive process as described in Heger et al. (2000). Magnetic fields may also transport angular momentum using, for example, the Spruit-Taylor dynamo (Spruit 2002) however it in unclear whether the process is active in massive stars (Zahn et al. 2007). We ignore possible chemical transport by the dynamo due to uncertainties about its validity. Rotational enhancements of the mass loss are also considered according to Langer (1997) where mass loss is enhanced as the star approaches the Ω-Limit with the formulation

$$\dot{M} = \dot{M}(V_{rot} = 0)\left(\frac{1}{1 - V/V_{crit}}\right)^{0.43}, \tag{1.17}$$

where

$$V_{crit} = \sqrt{\frac{GM}{R}(1 - \Gamma)} \tag{1.18}$$

and

$$\Gamma = \frac{\kappa L}{4\pi c G M}. \tag{1.19}$$

1.6.4 Treatment of mass loss

BEC employs a Lagrangian grid with mass coordinates (or isobaric coordinates in the case of rotating models). Near the surface however, mass loss depletes material from the surface of the star and to account for the change in the range of mass coordinates we switch to a pseudo-Lagrangian grid by dividing the mass coordinate with the total mass. As mass is lost near the surface, the angular momentum at that point is also subtracted so as to not violate the law of Conservation of Angular Momentum.

1.6.5 Other processes

In radiative zones, chemical changes occur via the process of radiative diffusion. Depending on the opacity and mass of each isotope, particles rise to the surface or sink deeper as they are accelerated by gravity and radiation pressure. Iron, for example, has a large opacity so during pre-core-collapse stages of evolution, it will rise upwards and create the iron convection zone. Other processes implemented are the various instabilities induced by rotation that lead to chemical mixing such as the Eddington-Sweet Circulation, the dynamical and secular shear instability, and the Goldreich-Schubert-Fricke instability (Heger et al. 2000).

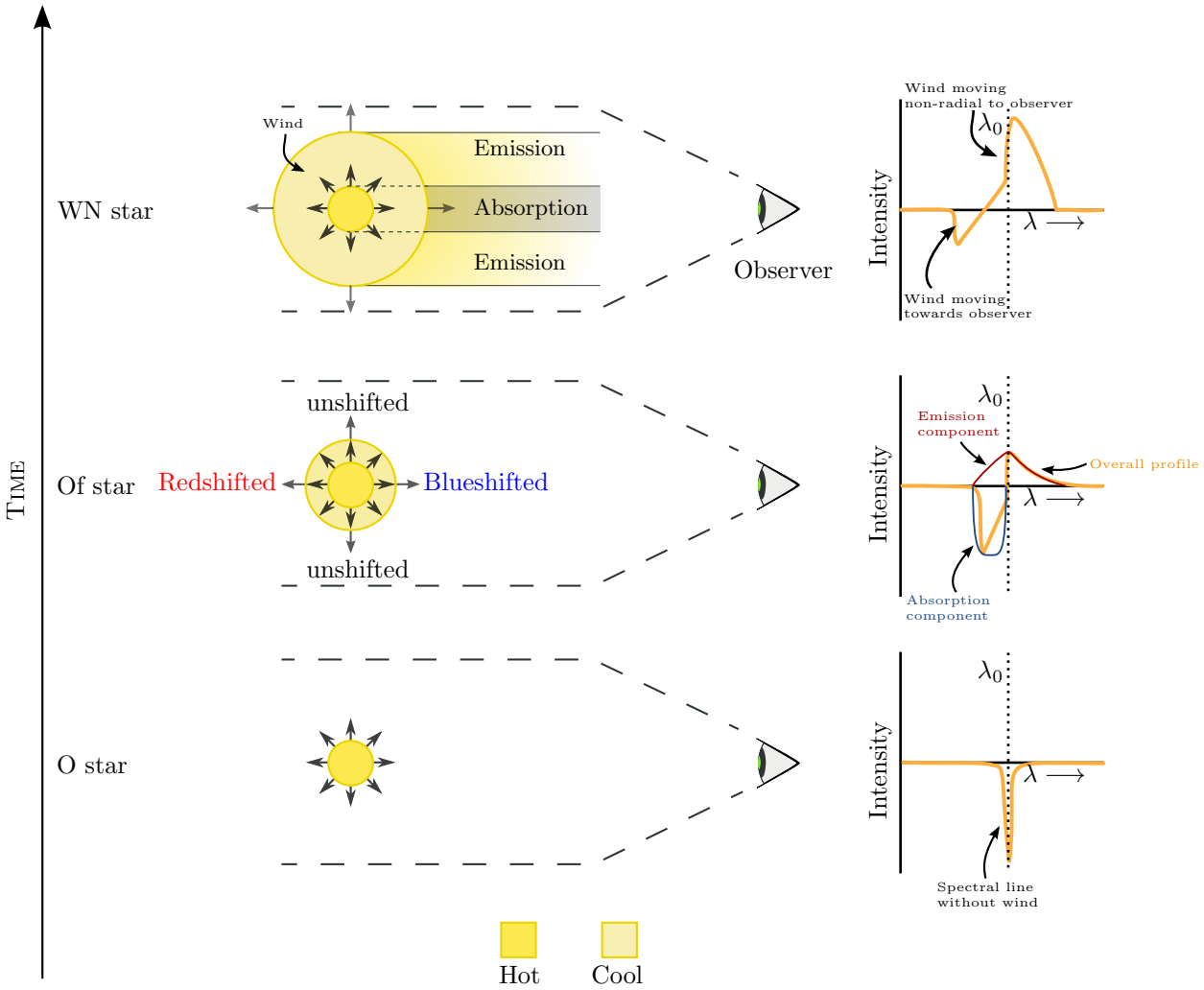

Fig. 1.4: A diagram showing the development of P-Cygni line profiles due to stellar winds. The star is initially a hot O star with no winds. Homogeneous winds create an extended envelope, part of which moves towards the observer which gives rise to blue-shifted absorption lines. The spectral lines of winds travelling non-radially to the observer are not shifted and as this gas is hot but not against a hotter background, emission lines are seen. This combination of blue-shifted absorption lines and emission lines is what produces a P-Cygni profile for stars with winds.

1.7 Mass loss of Massive Stars

1.7.1 OB/Of stars

Mass loss in main sequence massive stars was first discovered by Morton (1967) who measured the UV spectra of OB supergiants ϵ and ζ Orionis to find absorption lines with their wavelengths shortened with a corresponding doppler shift of $1900 kms^{-1}$. They concluded that this must be due to stellar winds and calculated a mass loss rate of 10^{-4} to 10^{-6} $M_{\odot}/yr$. Lucy & Solomon (1970) later attributed this to a net outward force accelerating ions from the atmosphere of the star. The ions later absorbed and emitted photons in a random direction with a particular doppler velocity, giving rise to the blue shifted absorption lines.

At these luminosities, stars come in several spectral types. Young stars begin their lifes as luminous O or less luminous

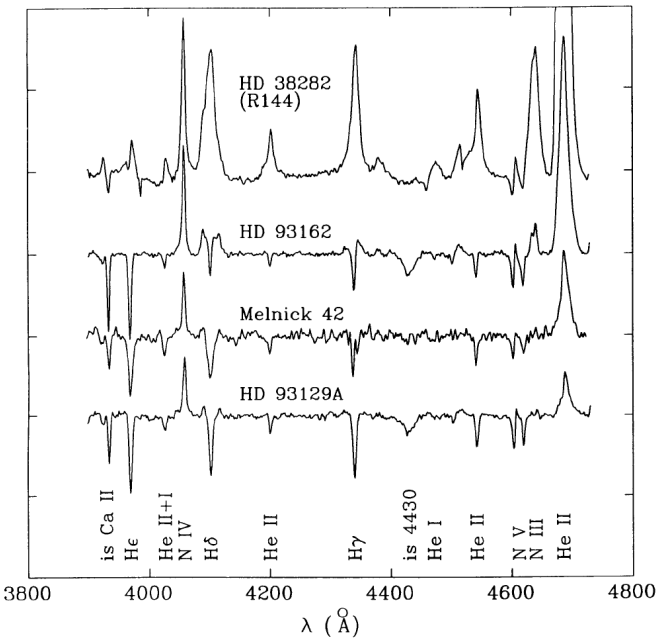

Fig. 1.5: Blue-violet spectrograms of stars in various stages of evolution. The increase in the intensity of emission lines may be attributed to the larger envelope and winds. From Walborn et al. (1992)

B dwarfs. Due to the presence of emission lines in their spectra, they may evolve into spectral type Of and later, a Wolf-Rayet star. Observations of these stars show a P-Cygni profile for spectral lines. A young O star initially exhibits only absorption lines due to the hot gas below the stellar envelope. Assuming that winds are accelerated homogeneously to create an extended envelope, the wavelength of absorption lines from winds that are moving towards the observer shorten due to the Doppler effect. Winds moving non-radially to the observer do not produce doppler shifted lines and because there is no hot gas behind them, they produce emission lines instead of absorption ones. When the two effects are combined, we get a P-Cygni profile. Over time, these winds get thicker so the intensity of the emission component increases (Figure 1.4). A spectral sequence of this process can be seen in Figure 1.5. When the surface hydrogen abundance reaches a critically low point, the star becomes a Wolf-Rayet initially with spectral classification WNLh when nitrogen lines dominate over carbon and strong hydrogen emission lines are present. It then moves progressively to WNL where hydrogen lines are weak, WNE in which hydrogen lines are absent, WC which shows stronger carbon lines than nitrogen and finally WO phases before the star explodes as a supernova.

The importance of these winds was realised and De Loore et al. (1977) calculated stellar evolution models of massive stars with mass loss rates scaled proportional to L. Subsequent work by Chiosi & Maeder (1986) included the correlation of $\dot{M}$ with M and R in addition to L. A major problem in this field is the calibration of the mass loss rate with observations. Due to observed clumping of the winds (Moffat 2008), empirical measurements of mass loss rates are made complicated. Theoretical modelling of the winds using hydrodynamic simulations (Abbott & Lucy 1985; Vink et al. 2001) include the treatment of radiative line driving but are also complicated by effects such as porosity (Muijres et al. 2010) and clumping as well as by the number of spectral lines that must be accounted for. In general, it is clear that the mass loss rates increase with increasing luminosity and metallicity (Langer 2012). This implication means that lower mass and

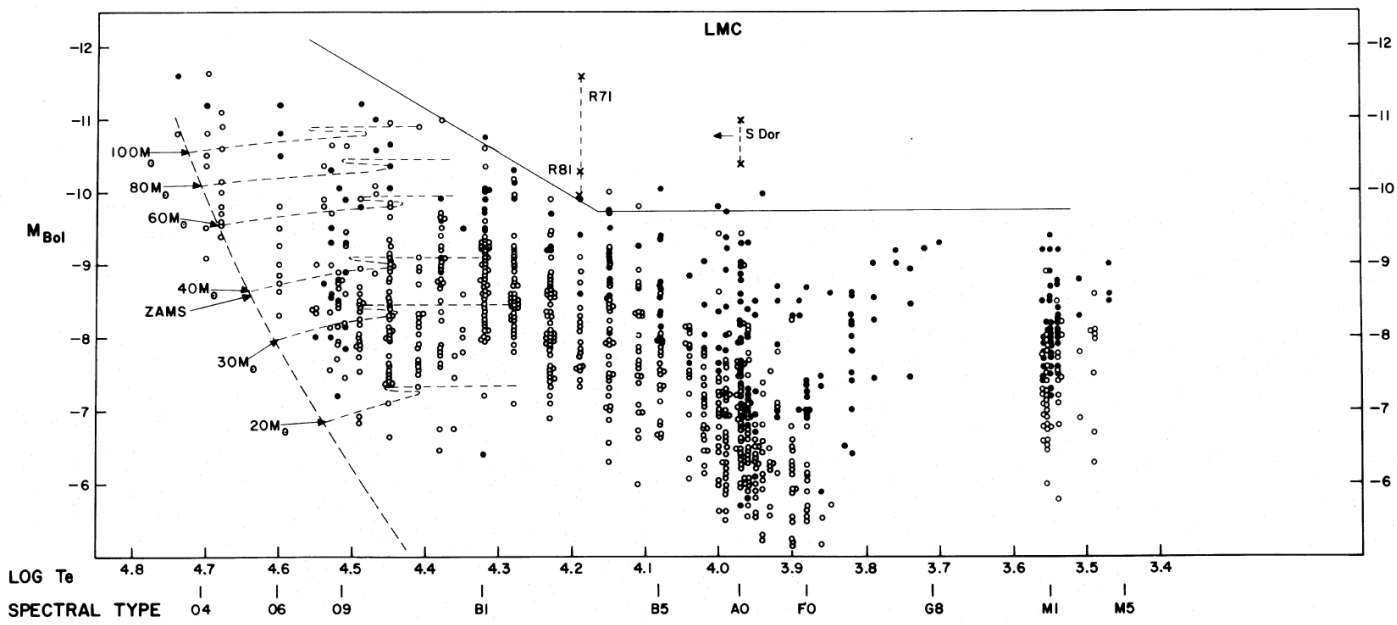

Fig. 1.6: An H-R diagram of massive stars in the LMC showing the Humphreys-Davidson limit (solid line). Dashed lines represent stellar evolution models. From Humphreys & Davidson (1979).

metallicity models (such as $M < 42M_{\odot}$ for the LMC) only lose a maximum of 10% of their mass on the main sequence due to winds (Brott et al. 2011) and therefore evolution models are not significantly affected.

While hydrodynamic wind models of these stars (Vink et al. 2011; Gräfener et al. 2011) have shown that these winds are generally driven by radiation pressure and identify the Eddington factor, Γ (where $\Gamma = \frac{L}{L_{edd}}$) as the most prevalent parameter for controlling mass loss, the mass loss rates calculated do not correlate well with the empirical rates, further highlighting the importance of porosity and clumping.

1.7.2 Humphreys-Davidson limit

Observations of the Galaxy, LMC and other locations have found there to be a lack of luminous red supergiant (RSG) stars. This upper limit is known as the Humphreys-Davidson (HD) limit after its discoverers Humphreys & Davidson. For the LMC (Figure 1.6), there are few stars with an effective temperature below $T = 14800K$ at luminosities above $log(L/L_{\odot}) = 5.83$, a trend that moves to higher temperatures with increasing luminosity. As can be seen in Figure 1.6, the few stars that are present in this region have been identified as Luminous Blue Variables (LBVs) which are thought to have periodic bursts of mass loss. More recent observations of the same and other regions of the universe confirm the existence of this limit so it is not an observational constraint. This HD limit is interpreted as a generalized Eddington limit and so stars near the boundary are thought to have high Eddington factors, driving mass loss. The understanding of the Humphreys-Davidson limit is a major motivation for this work.

1.7.3 Eddington mass loss

The Eddington limit is the limiting luminosity of a star at which point its outer layers begin to accelerate outwards. If this limit is passed, the envelope will begin to lose mass through stellar winds.

By assuming that all the momentum from photons are transferred to matter, we can get a maximum mass loss rate using (1.10):

$$\dot{M} v_\infty < \frac{L}{c} \tag{1.20}$$

where v_∞ is the terminal wind velocity at infinity. In reality, the mass loss rates will vary due to clumping, porosity and multi-scattering of photons (when the photon transfers its momentum to several ions). Multi-scattering becomes especially important when modelling optically thick Wolf-Rayet winds (Vink et al. 2011). We also need to consider that there are opacity peaks present near the surface of stars, such as the Iron, Helium and Hydrogen convection zones, all of which may create a peak in the Eddington factor below the surface of the star. This means that the luminosity in (1.20) should in fact be the fraction of the luminosity carried by photons, i.e., the radiative luminosity $L_{rad} = L\frac{\nabla}{\nabla_{rad}}$, because luminosity carried by convection or other means cannot drive a stellar wind. In this respect, there may be a secondary criterion for a high Eddington factor driving a wind. As mentioned in Langer (1997), a large Γ below the surface may drive convection and maintain stability rather than drive a wind.

If a large Eddington factor occurs at larger radii, where the density is too low for convection, it is also possible that radiative instabilities similar to Rayleigh-Taylor instabilities may be exhibited, which lead to "photon bubbles" (Spiegel & Zahn 1977). This reduces in the opacity of the layer, which in turn increases the local Eddington luminosity l_{edd}. Another possibility demonstrated by (Shaviv 2001) suggests that intrinsic instabilities are created, even in a gas supported fully by Thompson (electron) scattering, which leads to inhomogeneities, similar to excitations of strange mode pulsations (Glatzel 1994; Papaloizou et al. 1997). These inhomogeneities, in general, modify the ratio between the radiative flux and the radiative force, implying that the inhomogeneities damp the effect of a high Γ (Owoki & Shaviv 2012). In our work, we attempt to address this damping effect by defining an optical depth criteria for mass loss due to the Eddington limit.

1.7.4 Rotation and the Omega limit

The situation is made more complicated by the fact that most massive stars are also rotating which enhances mass loss further due to the Omega limit. For very fast rotators, rotational mixing drives chemically homogeneous evolution (abundances are isotropic) and these stars generally evolve along the Hayashi track on the H-R diagram and not near the Humphreys-Davidson limit (Köhler & Langer 2012; Brott et al. 2011) so we do not consider stars with $v_{surf} \gtrsim 350 kms^{-1}$. We assume that magnetic fields induce solid body rotation in our models to simplify simulations but this generally true for massive stars.

1.7.5 Later stages of evolution

According to Langer (2012), the late stages of evolution are defined by the initial mass of the star. Stars around $60M_{\odot}$ become spectral type Of at the end of the main sequence due to stellar winds. When the wind becomes optically thick, they transition to WNLs. Higher mass stars become Of and WNL at an earlier point in the main sequence evolution. All of these stars later transition into Luminous Blue Variables (LBVs), which come in two recognisable varieties: the cataclysmic η-Carinae type or the more docile and predictable S Doradus variables. The mechanisms for both types of LBVs are subject to current research. During the LBV stage, stars may make large horizontal movements on the HR diagram and may also cross the Humphreys-Davidson limit. Lower mass LBVs become WNEs with no hydrogen present while higher mass ones continue as WNLs until the end of their core helium burning phase. The stars evolve to WN and WC phases and later to WO (Figure 1.7 depicts this process as a diagram). Depending on their mass, they may explode as core collapse or pair instability supernovae. A particularly interesting feature of the latter case is that no remnant is left behind. While the evolutionary sequence described hinges on the mass of the star, the metallicity is also an important factor as it determines the effectiveness of radiative driving of the stellar winds. Our work was carried out with stars at an LMC metallicity.

1.7.6 Previous work

There is a lack of previous work in this particular subject area. A number of stellar evolution calculations of massive rotating stars with mass loss have been carried out in the past (Köhler & Langer 2012; Brott et al. 2011; Maeder & Meynet 2000, 2010). However, while they consider the effect of mass loss due to the Omega limit, none of the studies utilize a theoretical mass loss recipe which directly takes the Eddington limit into account. Alternate studies using hydrodynamic wind models have been carried out by Vink et al. (2000, 2011) and Gräfener et al. (2011). While these simulated the winds of massive stars well and the derived quantities for mass loss can be fed into evolutionary calculations (and they are), a simplified stellar structure was used which assumed homogenity near the surface and ignored the importance of sub-surface convection zones for winds. Furthermore, they do not explain the Humphreys-Davidson limit nor did they intend to. There have also been some older studies (Langer 1998) who originally proposed the idea of scaling mass loss with the Eddington limit. In general, however, this work is the furthest the idea has been taken.

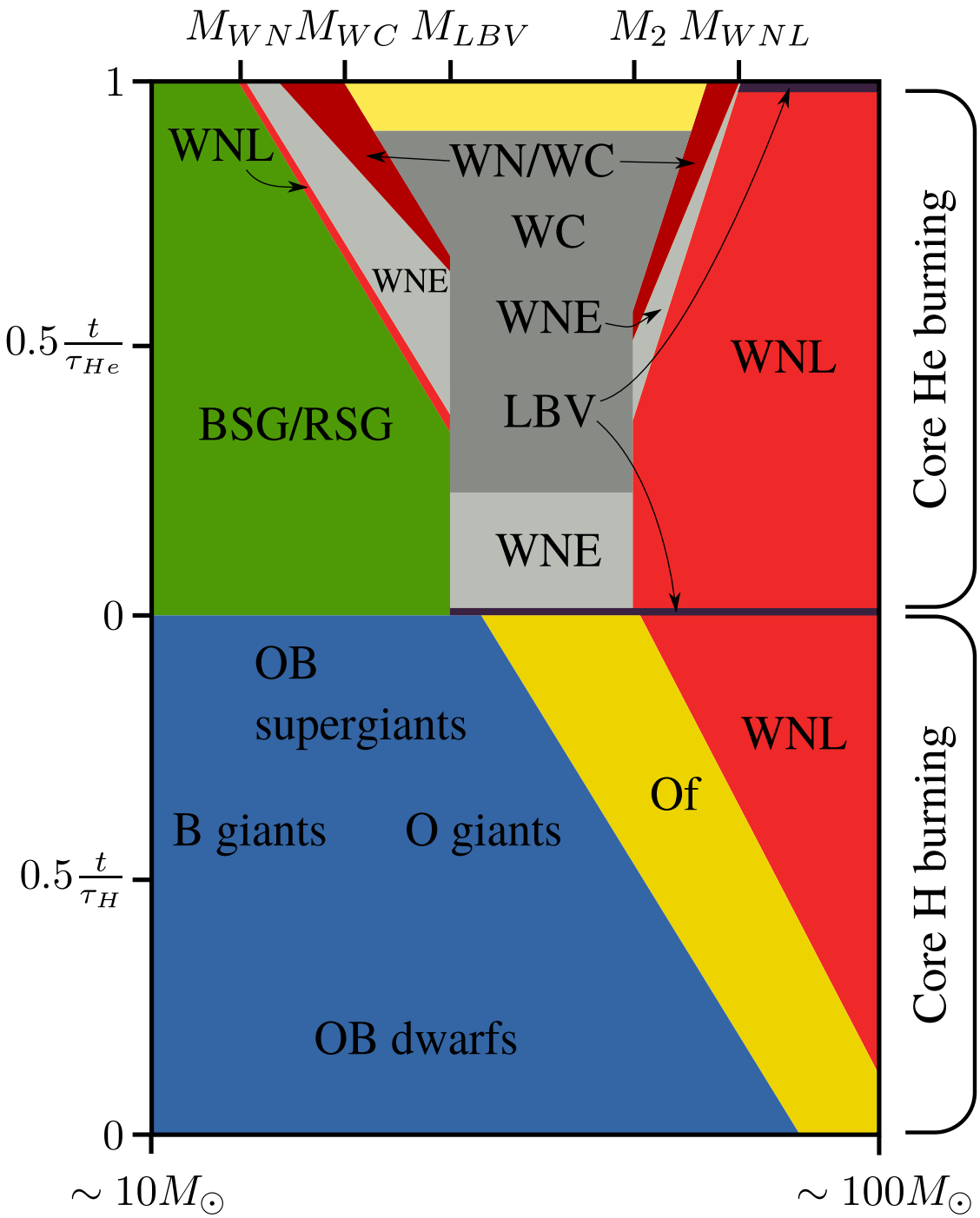

Fig. 1.7: A diagram showing the evolution of massive stars from $10M_\odot$ to $100M_\odot$ over the course of their Hydrogen and Helium main sequences. From Langer (2012)

Chapter 2

Simulations

2.1 Mass loss prescription

For our work, we utilize a mass loss prescription based on a combination of Vink et al. (2000, 2001), Nieuwenhuijzen & de Jager (1990) and Hamann et al. (1995), and scaled as a function of the Eddington factor. Vink et al. simulated wind models for a grid of OB stars with a range of luminosities and parameters and also considered the bi-stability jump (when the mass loss rate increases by a large factor due to the recombination of Fe IV to Fe II at the sonic point). The prescription was found to correlate well with observations of galactic stars presented in Mokiem et al. (2007a) as well as those of stars in R136 in the LMC (Yusof et al. 2010) within 0.2 dex for a surface helium abundance of around $Y_{surf} = 0.4$. As described in Brott et al. (2011), mass loss rates across the bi-stability jump were interpolated linearly rather than including the sharp increase in mass loss as presented by Vink et al. (2000). To match the increase in the mass loss rate as the star evolves to lower temperatures, the mass loss rate is switched to the empirical mass loss rates measured by Nieuwenhuijzen & de Jager (1990). This occurs when the Vink et al. (2000) rate becomes smaller than Nieuwenhuijzen & de Jager (1990) for temperatures below the critical temperature of the bi-stability jump (around $T_{surf} \approx 22.5kK$), ensuring a smooth transition from one to the other.
The above combination of Vink et al. (2000) and Nieuwenhuijzen & de Jager (1990) is then slowly transitioned into the empirical Wolf-Rayet mass loss rates presented in Hamann et al. (1995). While $0.4 \leq Y_{surf} \leq 0.7$, the Vink-Nieuwenhuijzen mass loss rate is interpolated with that of Wolf-Rayets in Hamann et al. (1995), reduced by a factor of 10 (Yoon et al. 2006). When the surface helium abundance increases to $Y_{surf} > 0.7$, we adopt the W-R rate of Hamann et al. (1995) completely.
We then consider the effect of the Eddington limit on the mass loss rate. Taking $\dot{M}_i$ as the mass loss rate calculated from the methods discussed previously, Γ is used to scale the rate as the star approaches the Eddington limit. Firstly, we need to define our value of Γ. At a particular point in time, $\Gamma(r)$ is seen to vary with radius and it is incorrect to assume that the largest value of Γ is right at the surface of the star. We therefore take Γ to be the maximum value of $\Gamma(r)$ in the star, a location that varies with time.

$$\dot{M}(\Gamma) = \dot{M}_i \left(\frac{1}{1-\Gamma}\right)^{\alpha} \tag{2.1}$$

where α is a free parameter. We limit the mass loss scaling to begin at $\Gamma \geq \Gamma_{min}$ and assume that it approaches a large number at $\Gamma = 1$. For a smooth transition from $\dot{M}_i to \dot{M}(\Gamma)$, we linearly interpolate between $\dot{M} = \dot{M}_i$ at $\Gamma = \Gamma_{min}$ and $\dot{M} = \dot{M}\Gamma$ at $\Gamma = 1$. The effect of this scaling is presented in Figure 2.1. In general, mass loss rates should only increase drastically as the star approaches $\Gamma = 1$ (Gräfener et al. 2011) which implies that the lower values of α are more realistic so in our models, we use a value of $\alpha = 0.2$. Due to precision errors, we were unable to choose a value of α too close to 0. Further more, we noticed that the effect of changing Γ_{min} was minimal so a value of $\Gamma_{min} = 0.9$ was assumed. The mass loss rate was limited to a maximum of $100\dot{M}_i$ to reduce numerical instabilities.

To account for the damping in the mass loss due to density inversions and instabilities (see Section 1.7.3), the enhanced mass loss rate was limited to when the optical depth at the maximum Eddington factor, τ_Γ, was less than a particular value τ_{max}. The optical depth, τ, is defined as

$$\tau(r) = \int_0^r \kappa dr \tag{2.2}$$

We initially settled on a value of $\tau_{max} = 30$, below which Eddington mass loss will occur. In Section 3.4, we considered the effect of a larger value of τ_{max}. The location of the maximum Eddington factor was observed to be in the layer above the shallowest subsurface convection zone. This is due to the peak in the opacity due to Fe, He or H which induces a large Eddington factor. Due to the initial temperature-initial mass relation for massive stars (Kippenhahn and Weigert), with increasing mass, the subsurface convection zones become shallower as the opacity peaks that produce them are highly temperature sensitive. This hints at the possibility of an upper limit to the initial mass $M_{ZAMS}(Z)$ for which Eddington mass loss is initially damped. When the stars evolve towards a lower effective temperature, the convection zones move deeper into the star and when they move to hotter effective temperatures, they rise up to the surface.

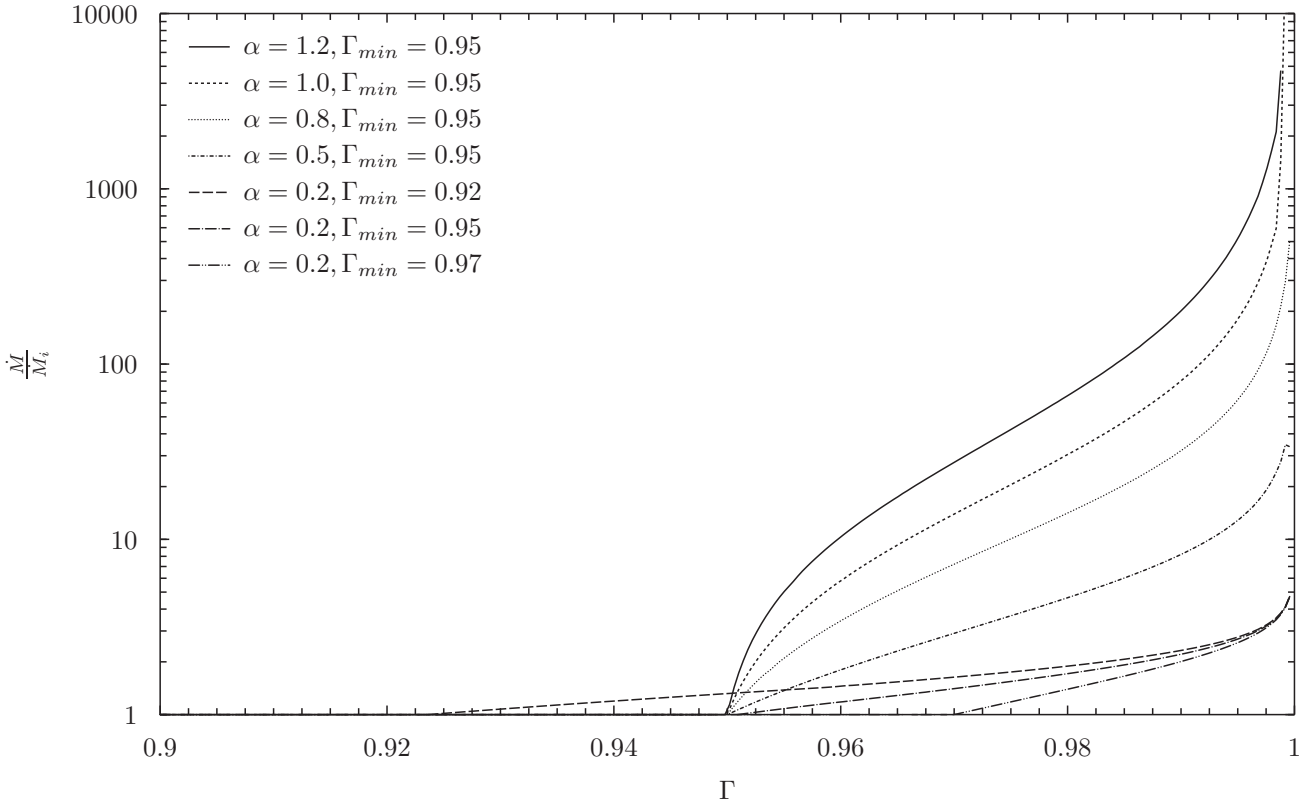

Fig. 2.1: An plot of the relative mass loss interpolated as a function of the Eddington factor for different values of α and Γ_{min}. There should only be a small amount of mass loss prior to $\Gamma = 1$ (Vink et al. 2011) so a small value of α was the optimal choice because of its steeper increase near $\Gamma = 1$. The choice of Γ_{min} appears to be less significant.

A rotating star has a lower effective gravity at its surface which may lead to more mass loss and to account for this, we reduced the Eddington limit from $\Gamma = 1$ to $\Gamma = \Gamma_{crit}$ when the layer with the maximum Eddington factor was rotating at a velocity v_{rot}.

$$\Omega = \frac{v_{rot}}{v_{crit}} \tag{2.3}$$

where

$${v_{crit}}^2 = \frac{GM}{R}(1 - \Gamma) \tag{2.4}$$

$\Omega = 1$ at $\Gamma = \Gamma_{crit}$. This gives:

$$v_{rot}^2 = v_{crit}^2 \tag{2.5}$$

After combining (2.4) with (2.5) and rearranging, we get

$$\Gamma_{crit} = 1 - f_{rot} \tag{2.6}$$

where $f_{rot} = {v_{rot}}^2 R/GM$.

We also included an additional linear scaling free parameter, b, for the mass loss rate to consider the effect of the wind efficiency η (Vink et al. 2000). $b \neq \eta$ but we may use it as an equivalent factor for the purpose of these models. Putting it all together:

$$\dot{M}(\Gamma) = \begin{cases} \dot{M}_i + \dot{M}_i \left[b \left(\frac{1}{\Gamma_{crit} - \Gamma} \right)^{\alpha} \left(\frac{\Gamma - \Gamma_{min}\Gamma_{crit}}{\Gamma_{crit} - \Gamma_{min}\Gamma_{crit}} \right) - \left(\frac{\Gamma - \Gamma_{min}\Gamma_{crit}}{\Gamma_{crit} - \Gamma_{min}\Gamma_{crit}} \right) \right] & \text{if } \tau_\Gamma < \tau_{max} \text{ and } \Gamma > \Gamma_{min}\Gamma_{crit} \\ \dot{M}_i & \text{otherwise} \end{cases}$$

We limited Γ to a maximum value just less than Γ_{crit} to prevent limit numerical instabilities in our simulations. The difference between the maximum value of Γ and Γ_{crit} was calculated in a way that the mass loss rate reached a maximum of $100\dot{M}_i$ before it was then linearly scaled with b.

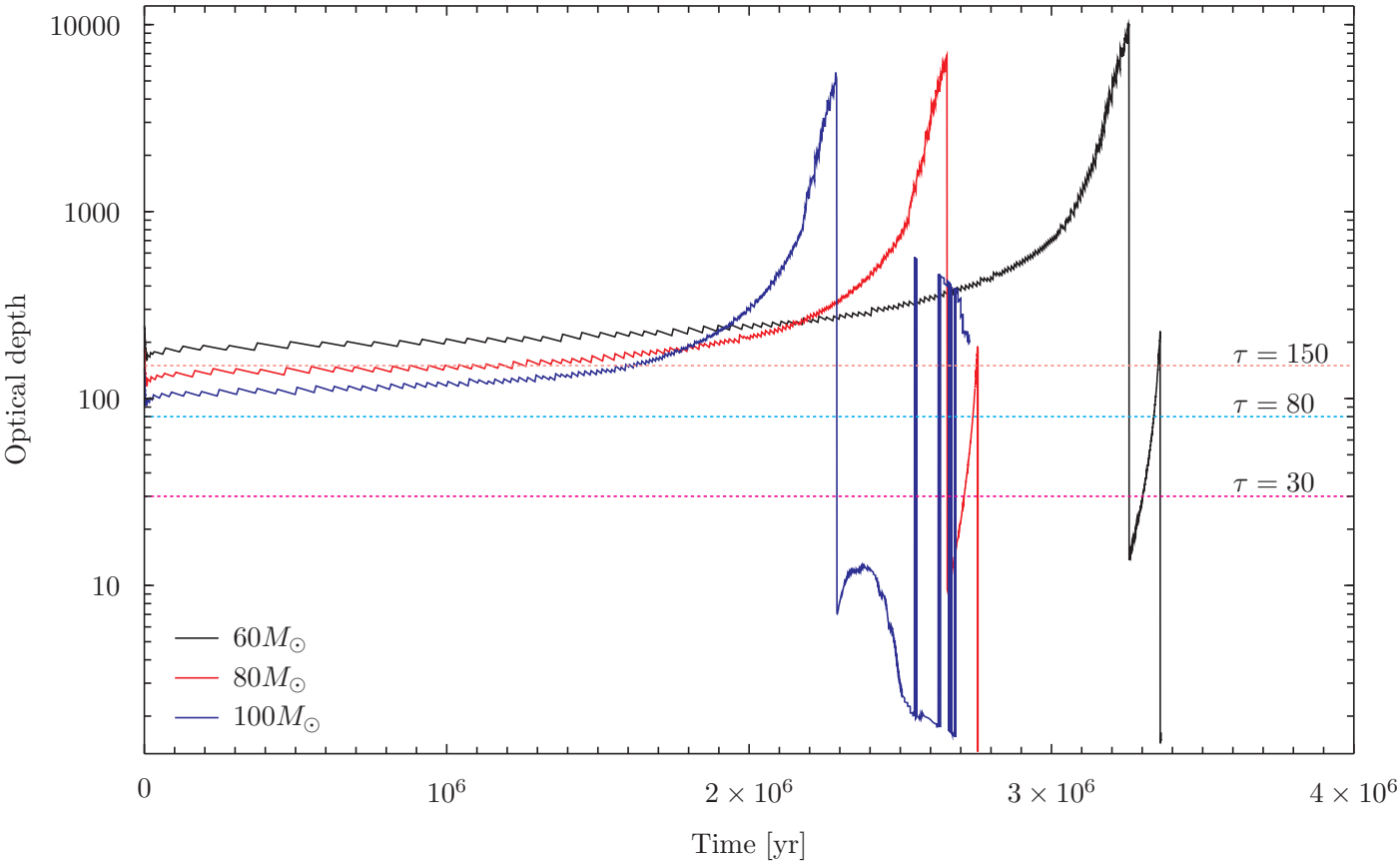

Fig. 2.2: The optical depth of the maximum Eddington factor over time for various initial masses. The Eddington factor generally peaks in the layer above the shallowest subsurface convection zone. With increasing stellar mass, these convection zones move closer to the surface due to the temperature sensitivity of the zone and the increasing initial internal temperatures of stars.

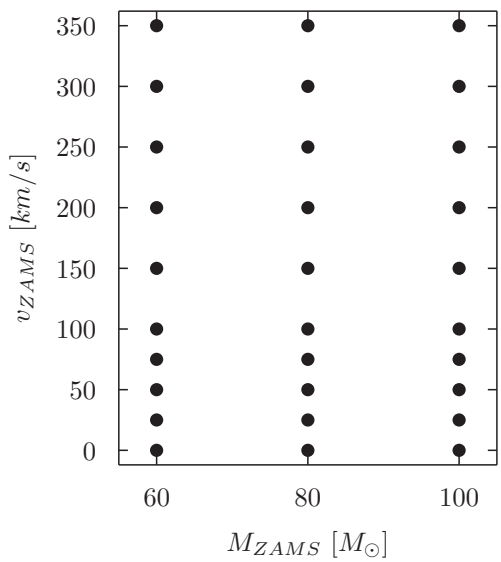

Fig. 2.3: The stellar evolution models that were calculated in this work.

2.2 Metallicity

For these models, an LMC metallicity was used. Rather than scaling chemical abundances from a solar metallicity, the initial abundances of C, N, O, Mg, Si and Fe were measured from observations of O and B stars in the LMC. Solar abundances were adopted for the rest of the heavy elements using data from Asplund et al. (2005), after scaling them down by 0.4 dex to account for the LMC. The abundance of Helium was calculated by assuming that it scales linearly between the primordial abundance ($Y = 0.2477$ at $Z = 0$) (Peimbert et al. 2007) and the solar abundance ($Y = 0.28$ at $Z = 0.012$) (Grevesse et al. 1996), giving us a value of $Y = 0.2562$. Our final chemical composition is $X = 0.7391$, $Y = 0.2562$ and $Z = 0.0047$. The opacity of the various elements was adopted from the infamous Opal opacity tables (Iglesias & Rogers 1996). Refer probablyto Brott et al. (2011) for more details.

2.3 Results

Stellar evolution models were calculated with masses in the range $60M_\odot$ - $100M_\odot$ and initial surface velocities between $0kms^{-1}$ - $350kms^{-1}$ using the following mass loss parameters: $\alpha = 0.2$, $\tau_{max} = 30$, $b = 1.0$, $\Gamma_{min} = 0.90$ (Figure 2.3). While we intended to run models until the end of core helium burning, we encountered a number of numerical difficulties associated with the large mass loss and the hydrodynamics of shells near the surface of the star. The majority of models presented are close to the end of core hydrogen burning with $X_{cen.} < 0.05$.
A selection of our models are plotted on a Hertzsprung-Russell diagram to show general trends (Figure 2.4). In the next chapter, we talk in detail about individual results and their implications.

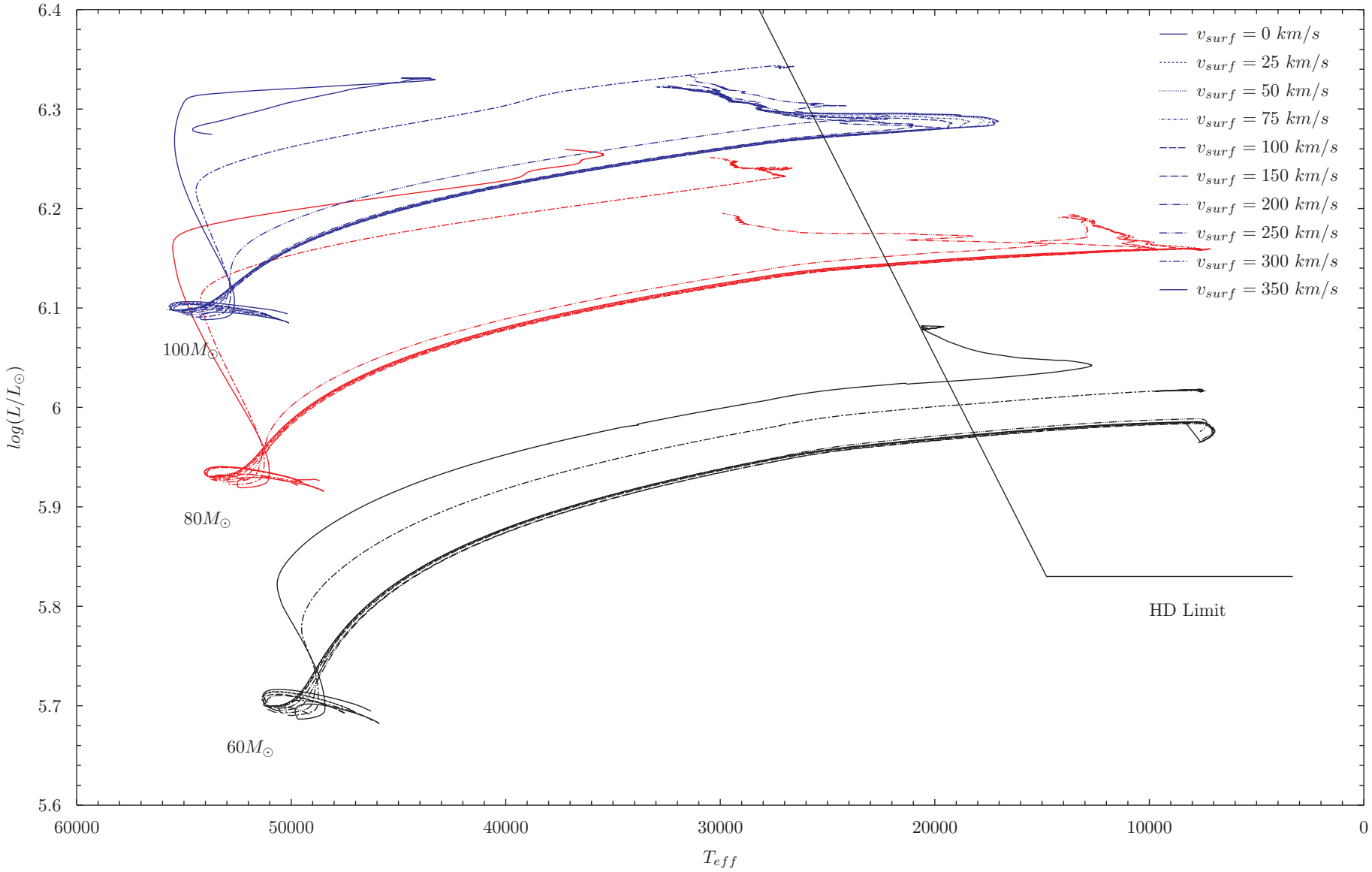

Fig. 2.4: A Hertzsprung-Russell diagram of our models. The surface temperature is plotted against the luminosity of the star to show evolutionary tracks. The Humphreys-Davidson limit is also plotted according to Humphreys & Davidson (1994)

Chapter 3

Discussion

A quick look at Figure 2.4 tells us a number of things. Unlike the evolution of low mass stars (the sun's luminosity increases by 0.75 dex during its main sequence), more massive stars evolve at an approximately constant luminosity for their main sequence lifetime. They also evolve to generally cooler surface temperatures during core hydrogen burning, again in contrast to sun-like stars. A contracting core will cause a larger increase in the radius due to the high temperature dependence of the CNO cycle- the radius of the non-rotating $60M_{\odot}$ model increases by factor of 500 whereas the radius of the Sun (which is powered by the p-p chain) will remain approximately constant for it's main sequence lifetime. Another clear trend is that the faster rotating models are cooler and bigger on the zero age main sequence, an effect caused by the centrifugal acceleration which inflates the envelope and reduces their effective temperature. Faster rotators also have larger convective cores which fuel the CNO cycle more efficiently and are subsequently more luminous. For the fastest rotating stars with $v_{surf} > 250\ km/s$, approximate chemically homogeneous evolution occurs. This causes helium ashes from hydrogen burning to reach the surface quickly, which in turn increases the luminosity due to the $L - \mu$ relation. In the HR diagram, these stars follow the Hayashi track for their evolution. Chemically homogeneous evolution occurs when the timescale for rotational mixing is larger than that of nuclear burning such that there is no chemical gradient between the core and the surface. As the star loses mass and therefore angular momentum, it spins down and the timescale for rotational mixing increases above nuclear burning. A chemical gradient begins to form in the star and the surface and core abundances decouple (Figure 3.1) which leads to the sudden redwards movement of the fastest rotating stars in the HR diagram. In Figure 3.2, a Kippenhahn diagram shows the evolution of the $100M_{\odot}$ model initially rotating at 350 km/s. Kippenhahn diagrams plot the internal structure of the star, including energy transport and generation, as a function of time.

It is clear that the the majority of models evolve beyond the Humphreys-Davidson limit. A preliminary estimate tells us that they spend on average a minimum of 154,000 years during the main sequence in this region with the actual time strongly depending on mass, surface velocity and mass loss parameters. Beyond the main sequence, the lower mass stars may also spend time in this region but due to the shorter timescales of nuclear burning, this is a maximum of 100,000 years. To study the density of stars in this region precisely and to compare it to observations, a population synthesis study is required. In this study, we instead concern ourselves with how well the various mass loss parameters may be used to describe the real Humphreys-Davidson limit.

In Figure 2.4 the faster rotating models appear to turn bluewards again at a hotter temperature than the slower rotators. This is especially visible with the $100M_{\odot}$ models and it tells us that rotation is an important effect that also influences the position of the Humphreys-Davidson limit. In the lower mass models, such as $60M_{\odot}$, rotation acts as a switch rather than a gradual effect. When Eddington mass loss occurs, the slow rotators are seen to decrease in luminosity while the fast rotators increase. This change occurs at around an initial velocity of $v_{surf} = 250\ km/s$ for $60M_{\odot}$ which is not coincidentally also the point at which models begin to evolve chemically homogeneously. Rotational mixing reduces the surface abundance of hydrogen at a faster rate and also creates a chemical gradient within the star. Rotation also keeps the star hotter (reduces T_{eff}) and when Eddington mass loss occurs, X_{surf} is lower than for slow rotators. Mass loss peels off the surface layers of the star which reveals layers with decreasing X. Since the electron scattering opacity $\kappa_{e.s.} \propto 0.19(1 + X)$, deeper layers have a lower opacity and therefore the luminosity of the star increases. At the same time, the radius of the star is decreasing but not sufficiently to reduce the stellar luminosity. In the case of slow rotators, Eddington mass loss occurs early and there is a plateau in the chemical gradient near the surface of the star (Figure 3.3). Removing the other layers through mass loss therefore does not lead to a reduced opacity so the star decreases in luminosity due to the reduced stellar radius according to the Stefan-Boltzmann law $L \propto R^2T^4$.

The initial rotation of the star is seen to correlate with the temperature at which the star turns bluewards. Figure 3.4 shows this property, which is not very clearly seen on the Hertzsprung-Russell diagram.

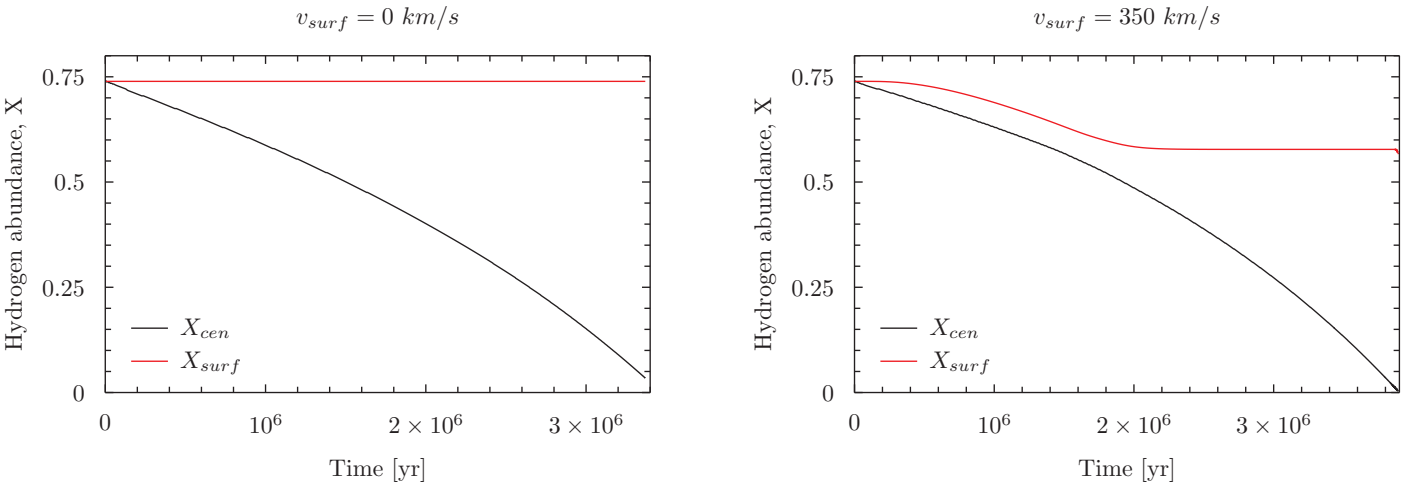

Fig. 3.1: Plots of the hydrogen abundances of the core and the surface of two $60M_\odot$ models. The left panel shows the change in abundance for a non rotating star (no rotational mixing) and the right panel shows a fast rotating star ($v_{surf} = 350\ km/s$). With the non rotating star, the surface hydrogen abundance does not decrease noticeably and only very slightly when rapid mass loss occurs at the very end. However, in the fast rotating star, rotational mixing makes the surface hydrogen abundance decrease proportional to the core hydrogen abundance. At around two million years, this proportionality stops because the star has spun down enough that the timescale for rotational mixing is larger than that for nuclear burning and so the surface abundance plateaus until rapid mass kicks in later.

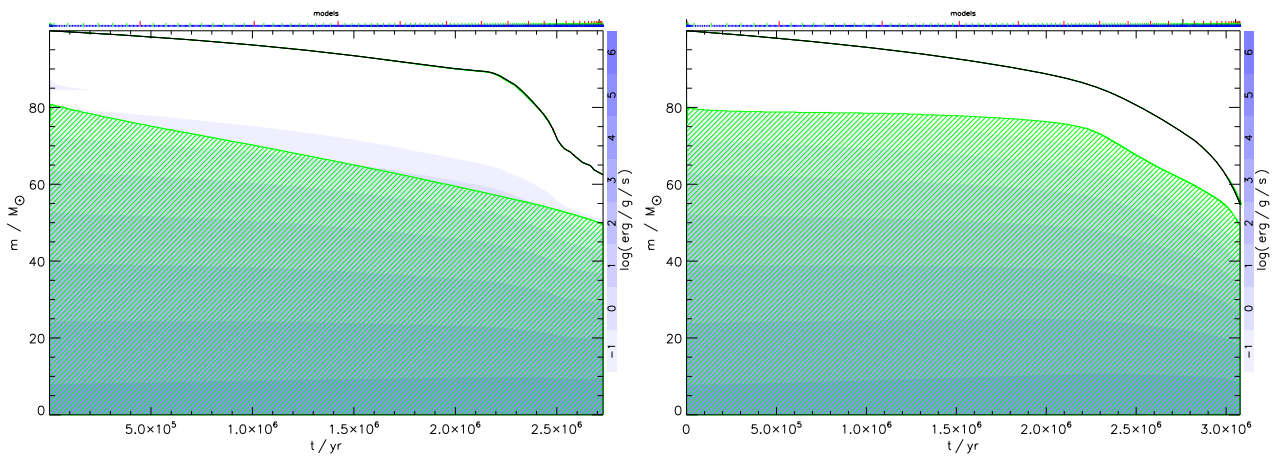

Fig. 3.2: Kippenhahn diagrams of $100M_\odot$ non-rotating (left) and fast-rotating (350 km/s, right) models. A Kippenhahn diagram shows the internal structure of the star as a function of time. The green striped area represents convection and the shades of blue represent energy generation. The boundary at the top of the diagram is the total mass of the star, which decreases slowly at first but rapidly when Eddington mass loss occurs. The fast rotating star has a much more massive convective core which drives mixing and prolongs the main sequence life of the star and make it more luminous.

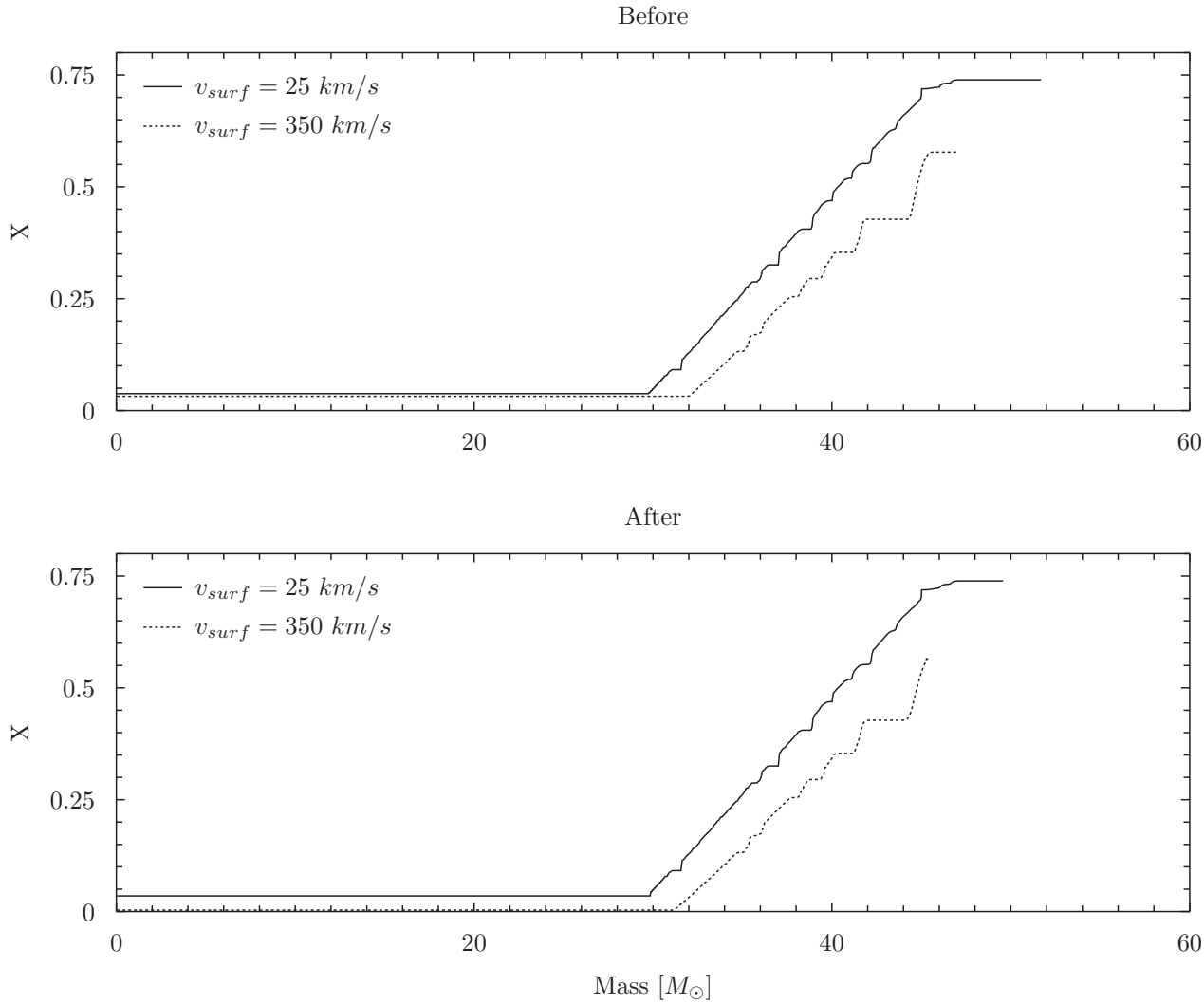

Fig. 3.3: The two panels show the hydrogen abundance of two stars rotating at different velocities prior to and after Eddington mass loss as a function of mass of the star. In the slow rotator, there is a large plateau in the abundance near the surface which means that when mass loss occurs, the revealed layers will not be of a lower abundance so the opacity does not decrease and the luminosity does not subsequently increase. This is contrary to the fast rotator which does show a decreasing abundance when mass is lost so the removal of layers will lead to a decrease in the opacity. This explains the fact that slow rotators decrease in luminosity while fast rotators increase when Eddington mass loss occurs

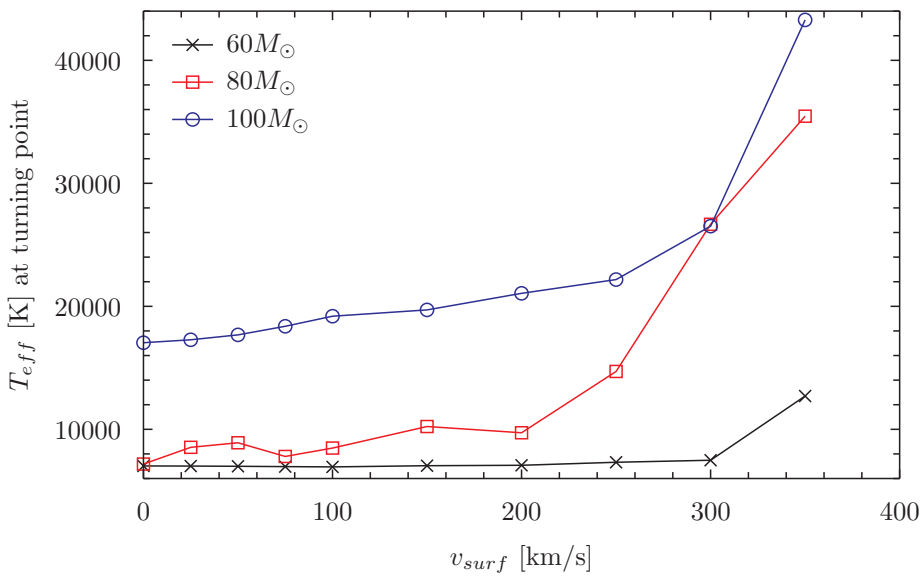

Fig. 3.4: A plot of the coolest temperature that the model reaches as a function of initial velocity. There is a clear link between the initial rotation rate of the star and the point at which the star turns bluewards due to Eddington mass loss. Lower masses and slower rotating stars turn at cooler temperatures.

3.1 $60M_\odot$ models

$60M_\odot$ models are not significantly affected by Eddington mass loss. They evolve past the Humphreys-Davidson limit relatively later than higher mass stars ($X_{cen} = 0.067$ for $60M_\odot$ compared to $X_{cen} = 0.182$ for $100M_\odot$ non rotating models at the limit) and do not turn bluewards quickly when mass loss does occur. This may be attributed to the fact that $\dot{T_{eff}}$ is larger for the lower mass stars stars and when the Helium convection zone forms at around $T_{eff} = 18,000\ K$ and triggers Eddington mass loss, the stars have enough "momentum" to continue of their redwards trajectory, causing the convection zone to move deeper than $\tau = \tau_{max}$ and disrupt Eddington mass loss. Faster rotators have a lower $\dot{T_{eff}}$ (Figure 3.5) and trigger Eddington mass loss for a longer period of time (Figure 3.6). In models with initial velocity $v_{surf} < 300\ km/s$, the stars were cool enough that a Hydrogen convection zone formed (Figure 3.7), triggering further Eddington mass loss. However, the main sequence was almost over and it was too late for the star to move bluewards again. After the main sequence, the helium core will contract which causes the envelope to expand due to the Virial theorem so star may move further redwards unless mass loss is strong enough to prevent it.

Considering Figure 3.8 where the relative Eddington factor ($\frac{\Gamma}{\Gamma_{crit}}$) is plotted against time, a few trends are noticeable. Firstly, the proximity to the Eddington limit (at $\Gamma = \Gamma_{crit}$) increases with initial velocity. This means that stars with velocity $v_{surf} \geq 150\ km/s$ reach the Eddington limit early in their evolution and do not have Eddington mass loss because we assume that mass loss does not occur for $\tau > \tau_{max}$. Later, due to the application of the Nieuwenhuijzen & de Jager (1990) mass loss rate for cooler stars, they move to lower Eddington factors and only then does Eddington mass loss occur and only for a short period, as discussed previously.

In Figure 3.9, we see the effect of mass loss on the Eddington factor as Eddington mass loss is applied for the $60M_\odot$ star rotating at $v_{surf} = 50\ km/s$. The graph is cropped to beyond three million years of evolution. The star initially has a trajectory of decreasing Eddington factor which was due to the Nieuwenhuijzen & de Jager (1990) mass loss rate. When Eddington mass loss is applied at $t = 3.26 \times 10^6$ years, it quickly begins to move towards the Eddington limit. When the Eddington mass loss is turned off at $t = 3.31 \times 10^6$ years, the star continues towards the Eddington limit and is accelerated when the second phase of Eddington mass loss occurs. After 10,000 years, this phase subsides and the star is seen to move away from the Eddington limit. It is at this point that the simulation crashes and we were unable to progress further. We originally intended for the mass loss to move the star away from the Eddington limit but that is clearly not the case in this model or even for the broader group of $60M_\odot$ stars (Figure 3.8).

Furthermore, none of the $60M_\odot$ evolved sufficiently bluewards to move out of the Humphreys-Davidson region which is a major shortcoming of this particular mass loss prescription. The fastest rotating models with partially chemically homogeneous evolution (as defined by Köhler & Langer (2012)) did have some success and the model initially rotating at $v_{surf} = 350\ km/s$ ended its main sequence life on the blue side of the Humphreys-Davidson limit (Figure 3.10). However,

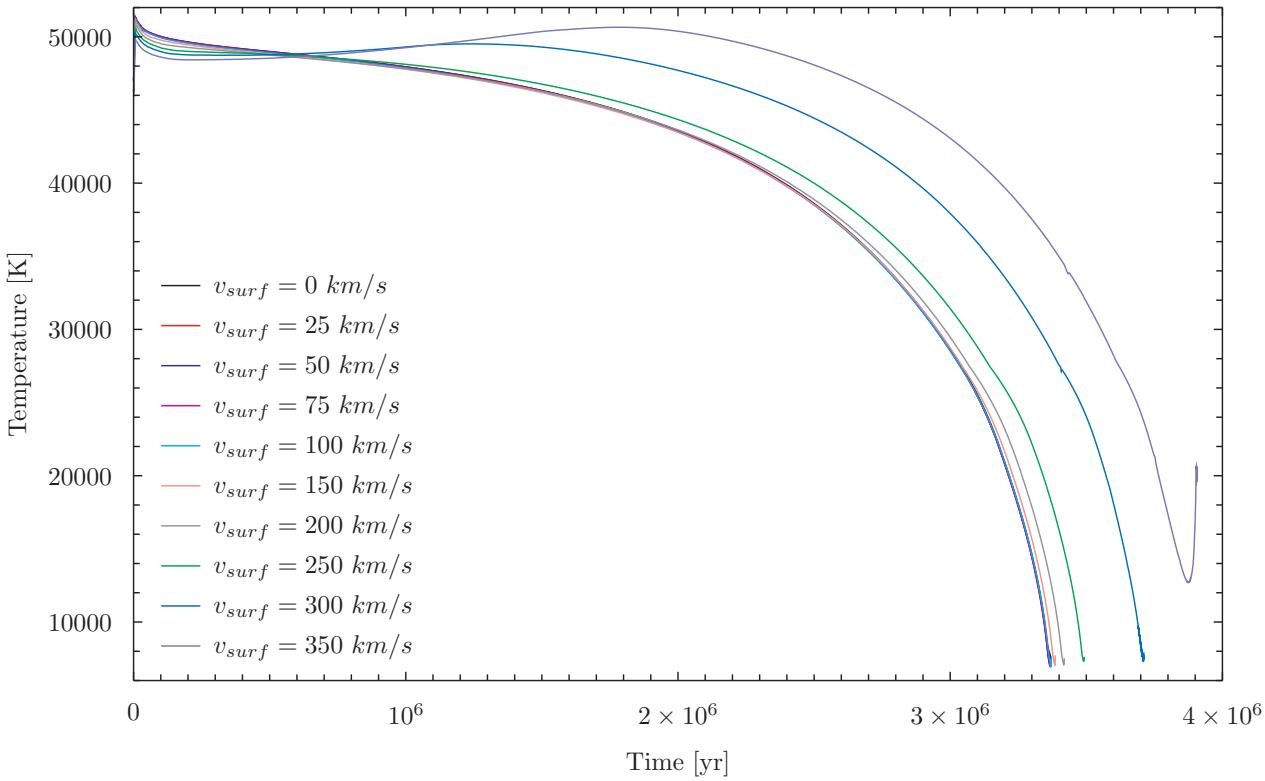

Fig. 3.5: A plot of the surface temperature of the star against time for $60M_\odot$ models. The faster rotators initially have a cooler surface temperature but their large rotationally mixed cores deter contraction of the core and therefore prevent the envelope from expanding quickly to cooler temperatures. Subsequently, they have a lower $\dot{T_{eff}}$ than slow rotators.

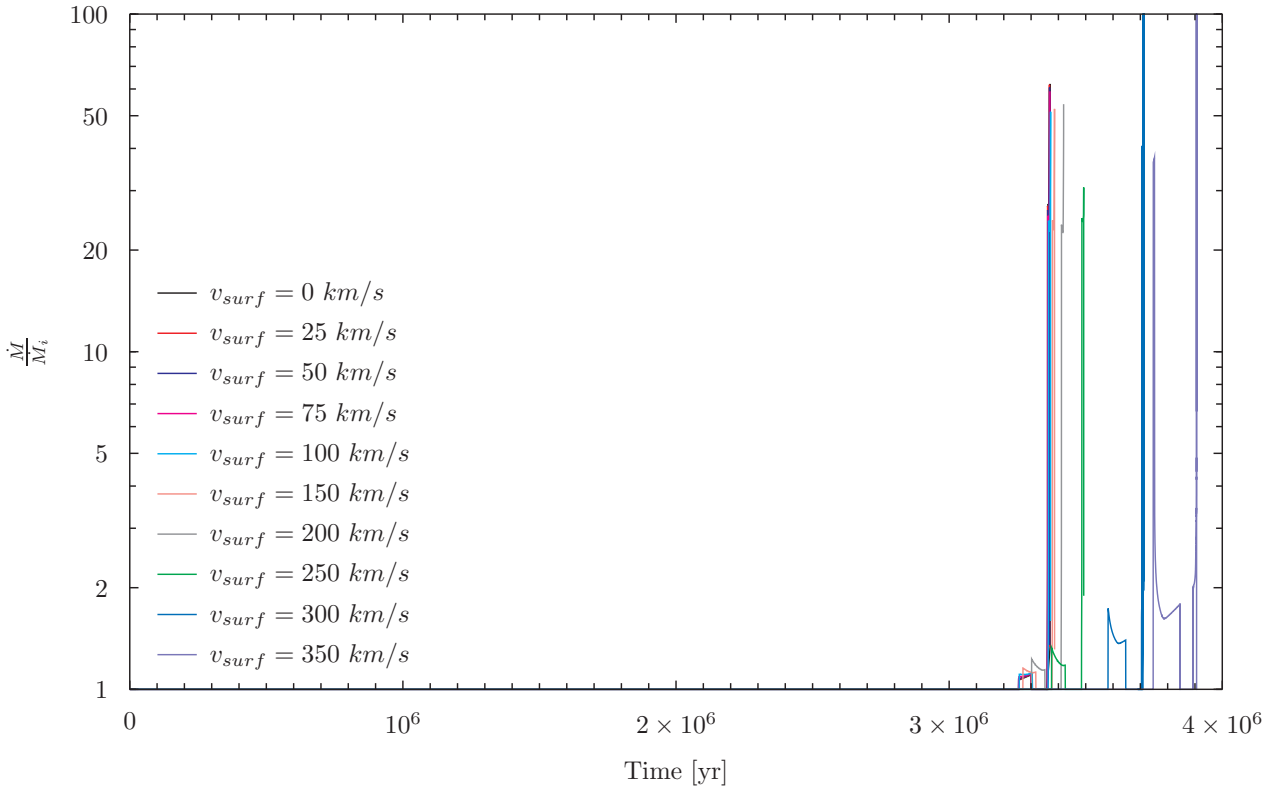

Fig. 3.6: The relative mass loss rate of the star as a function of time for $60M_\odot$ models. Note the logarithmic y axis. We chose a relative mass loss rate because it allows us to clearly see where Eddington mass loss is applied. The period of mass loss is greater for faster rotators due to their slower redwards movement.

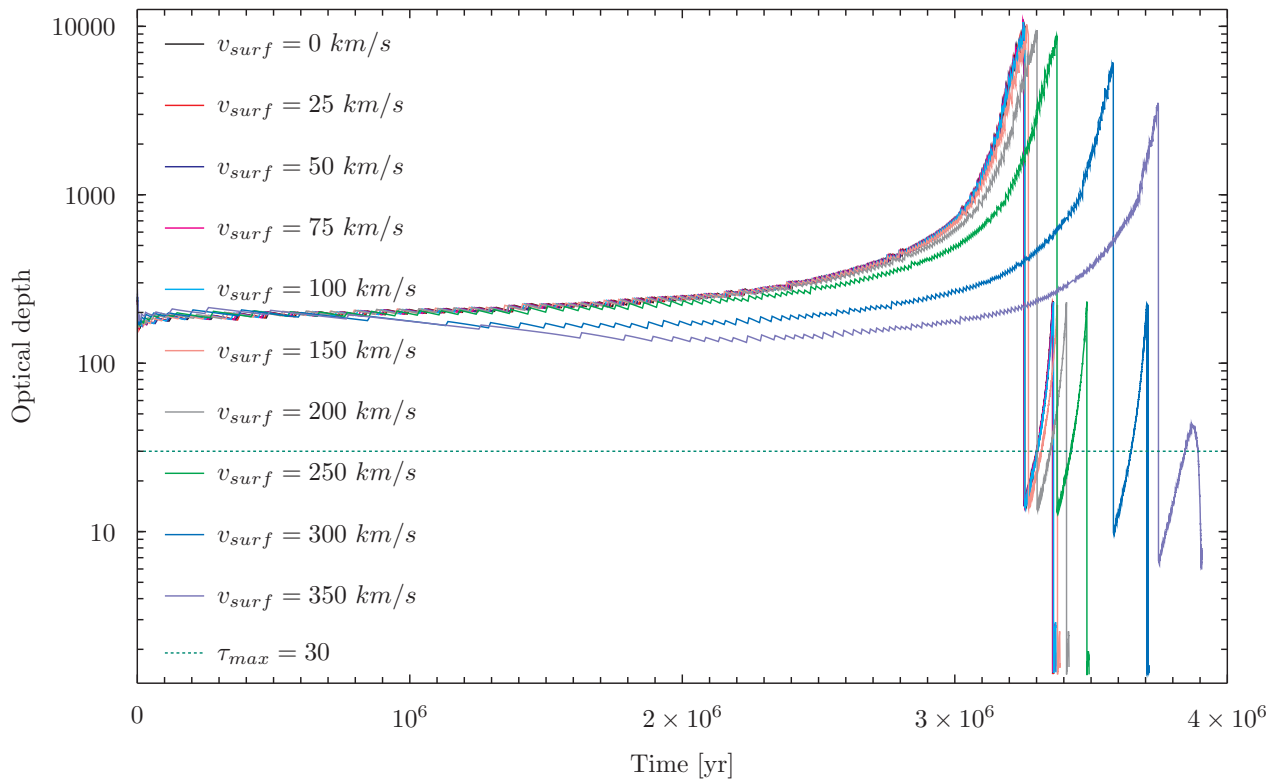

Fig. 3.7: The optical depth of the maximum Eddington factor as a function of time for $60M_{\odot}$ models. Near the end of main sequence evolution for the slower rotators, the maximum Eddington factor jumps very close to the surface as seen by the low optical depth. This is due to the formation of a Hydrogen convection zone because of the cool temperature of the star. Faster rotators are hotter and may turn bluewards before they reach such a temperature. In the $v_{surf} = 350\ km/s$ model, we do not see the formation of a Hydrogen convection zone but instead, the optical depth of the maximum Eddington factor stays in the Helium convection zone as it moves to hotter temperatures and the zone climbs to the surface.

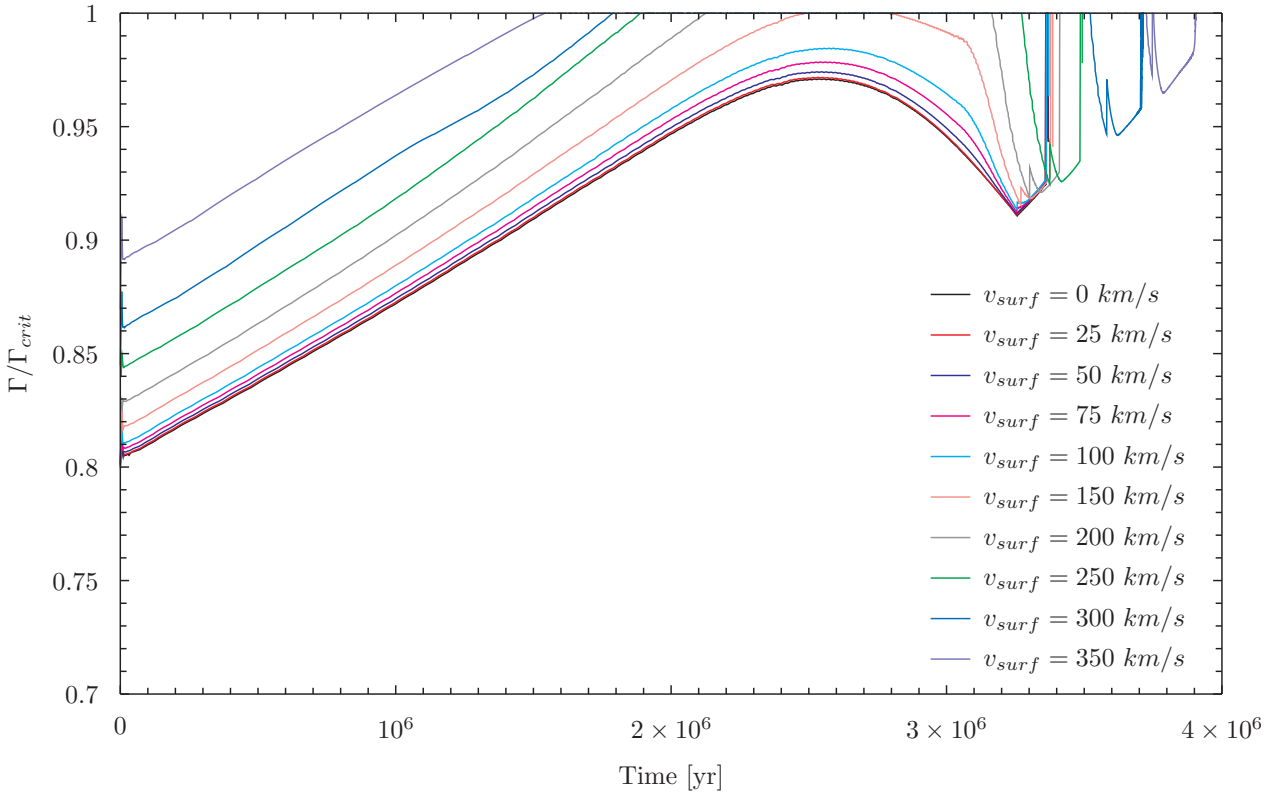

Fig. 3.8: The change in the Eddington factor as a function of time. Eddington mass loss moves the star towards the Eddington limit at the top of the graph. Faster rotating models evolve with larger values of Γ

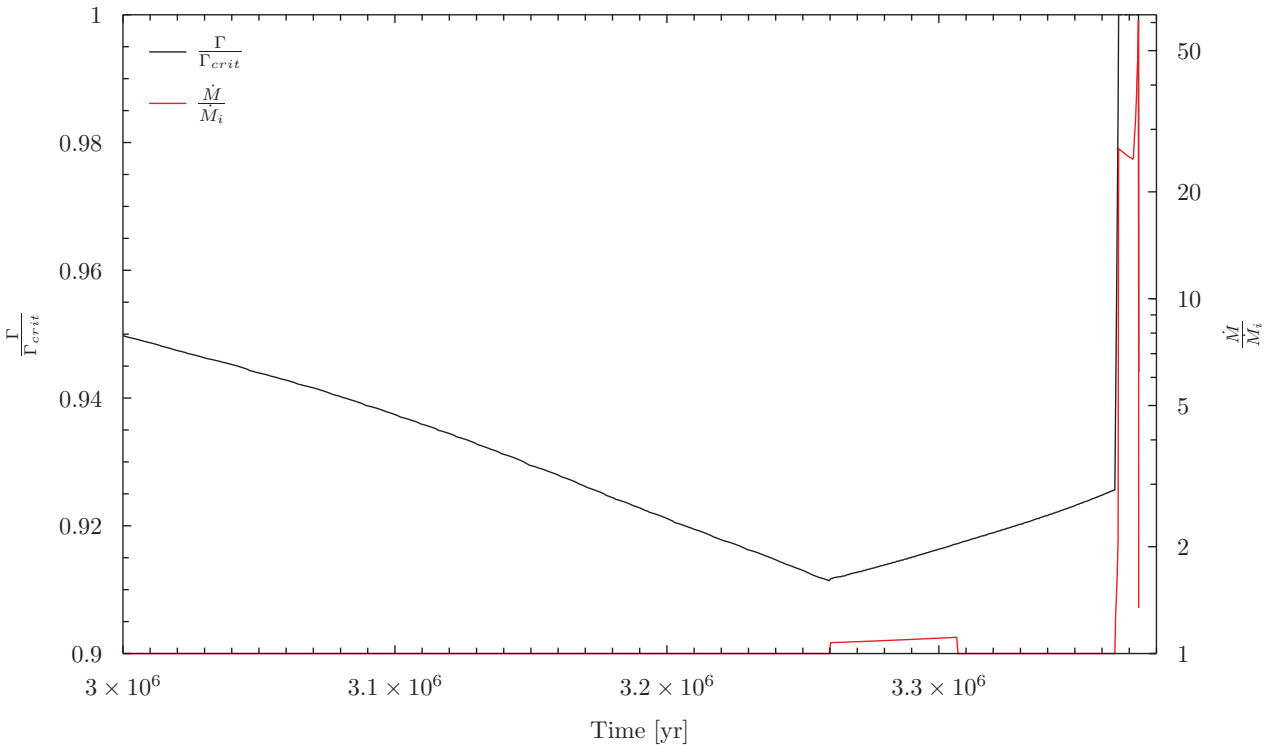

Fig. 3.9: Relative mass loss rate and Eddington factor as a function of time for a $60 M_{\odot}$ star rotating slowly at $v_{surf} = 50\ km/s$. Note that the time begins three million years after the ZAMS.

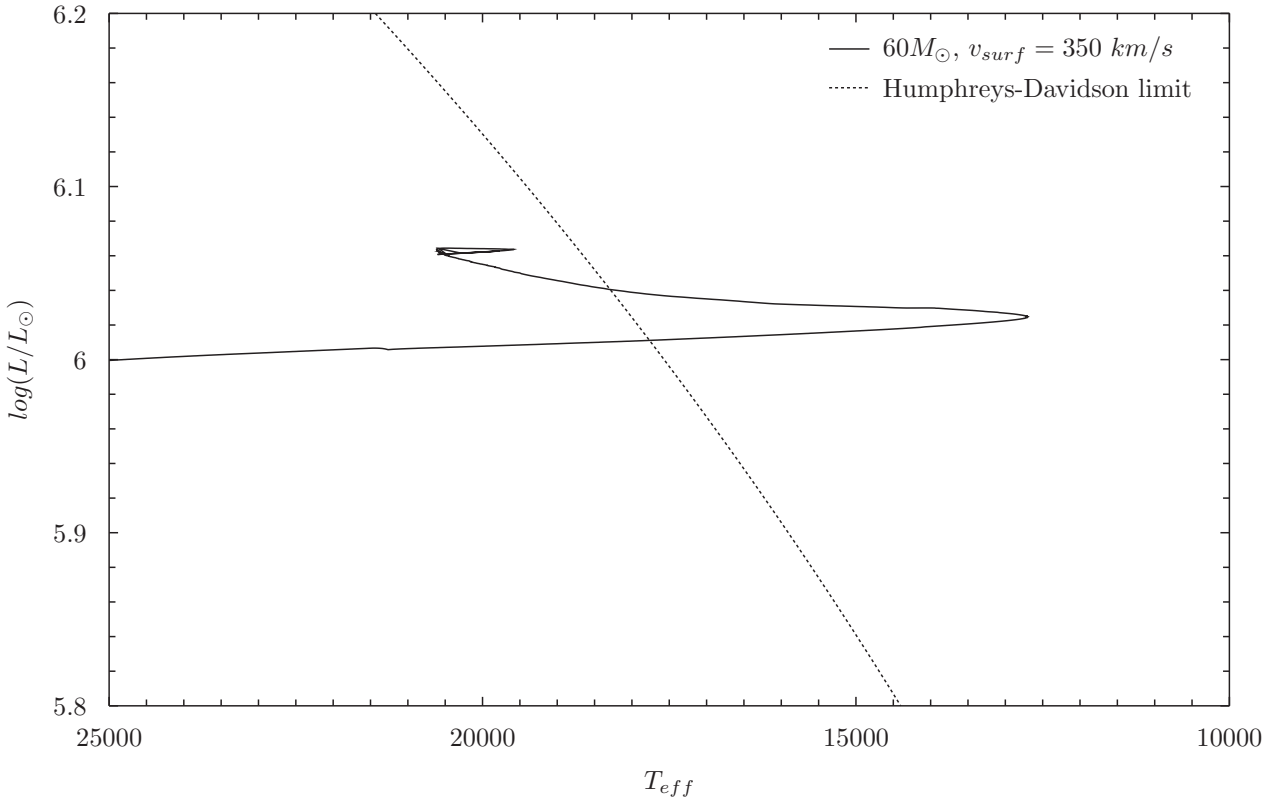

Fig. 3.10: A zoomed in plot of the Hertzsprung-Russell diagram of the $60M_\odot$ star initially rotating rapidly at $v_{surf} = 350\ km/s$. The star ends its main sequence on the blue side of the Humphreys-Davidson limit, unlike slower rotating $60M_\odot$ models, because its Eddington mass loss is larger due to its lower T_{eff} and $\dot{\tau}$ (Figure 3.7).

Brott et al. (2011); Hunter et al. (2008) find that the initial velocity distribution for B-type stars with $M \leq 25M_\odot$ in the LMC peaks at $v_{surf} = 100\ km/s$ so if we assume that the distribution is similar for higher mass O-type stars, the tracks of fast rotators are probably more the exception than the rule and a better prescription describing slow rotators is also required.

Figure 3.11 shows the rotational parameter f_{rot} as a function of time for the $60M_\odot$ models. We note that $f_{rot} \propto v_{rot}^2$ so doubling the initial velocity quadruples f_{rot} and therefore the mass loss is much stronger. The general increase in f_{rot} over time is due to the expansion of the star while mass loss at a later stage spins the star down due to a loss of angular momentum and therefore the effect of the rotation on the mass loss generally decreases in time. After the second phase of Eddington mass loss, f_{rot} is unlikely to be a large quantity and rotational effects on mass loss may be safely ignored.

We also note that all of the models spin down completely before the end of the main sequence (Figure 3.12). Observationally, this means that stars may be identified with similar rotational periods and masses (Figure 3.13) but different surface chemical abundances and other stellar properties. In Figure 3.14, we see that the surface abundances of Hydrogen may vary by at least 15% depending on the initial rotation of the star. The graph also highlights the fact that Eddington mass loss is quite insignificant in depleting hydrogen from surface of these models during the main sequence and significant depletion is only achieved in the fastest rotators. However, to correlate with observations of low mass Wolf-Rayet stars, mass loss must continue beyond the main sequence, and lead to further depletion of hydrogen.

In general, it is clear that for $60M_\odot$ stars, the current Eddington mass loss prescription with mass loss parameters $\alpha = 0.2$, $\tau_{max} = 30$, $b = 1.0$, $\Gamma_{min} = 0.90$ is not sufficient to describe the Humphreys-Davidson limit. Modifying the optical depth parameter τ_{max} leads to a longer period of mass loss (Section 3.4). Similarly, by changing b and scaling the mass loss, the turning point of these models may be influenced (Section 3.5.

3.2 $80M_\odot$ models

$80M_\odot$ models were more significantly affected by Eddington mass loss. Due to the closer proximity to the Eddington limit (Figure 3.15), the relative mass loss rates of these stars are larger. They also reach the Humphreys-Davidson limit earlier

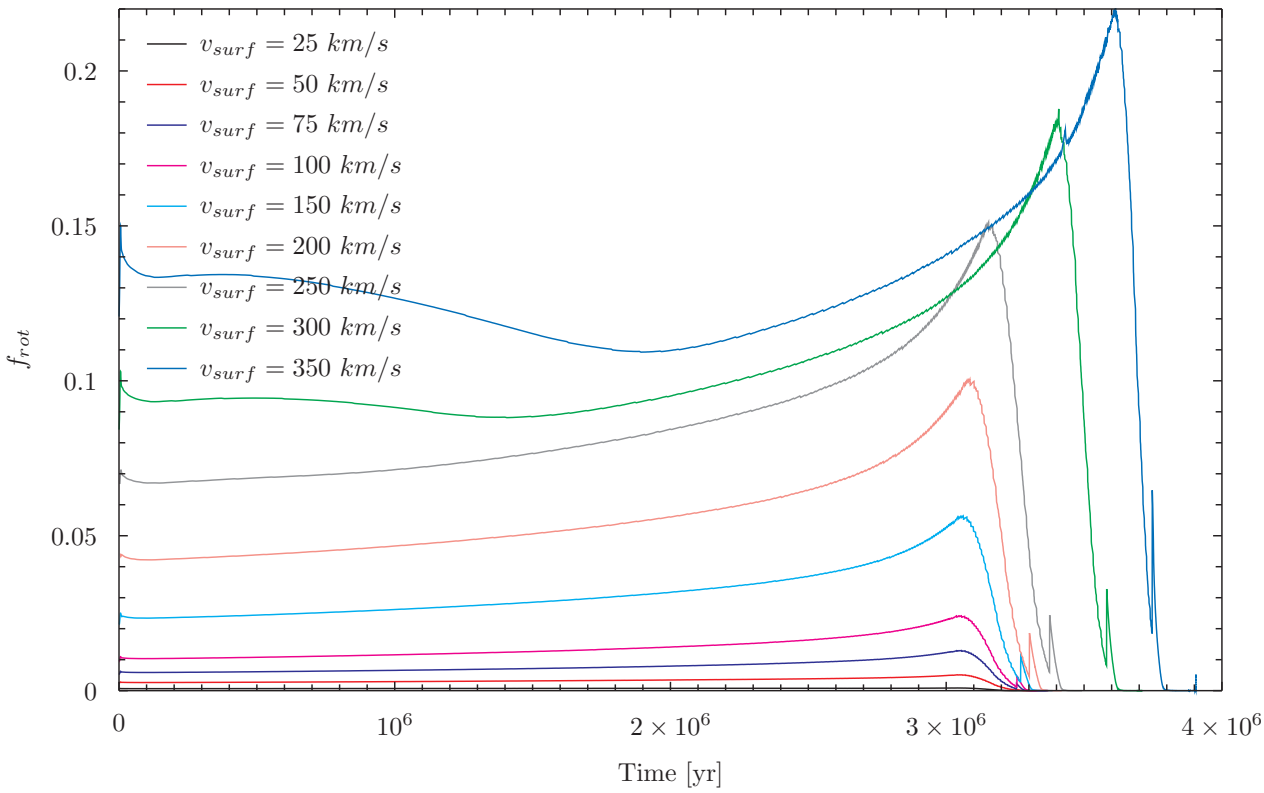

Fig. 3.11: The change in the rotational parameter f_{rot} over time for $60M_\odot$ models. A large decrease occurs when Eddington mass loss kicks in near the end of the models' main sequences.

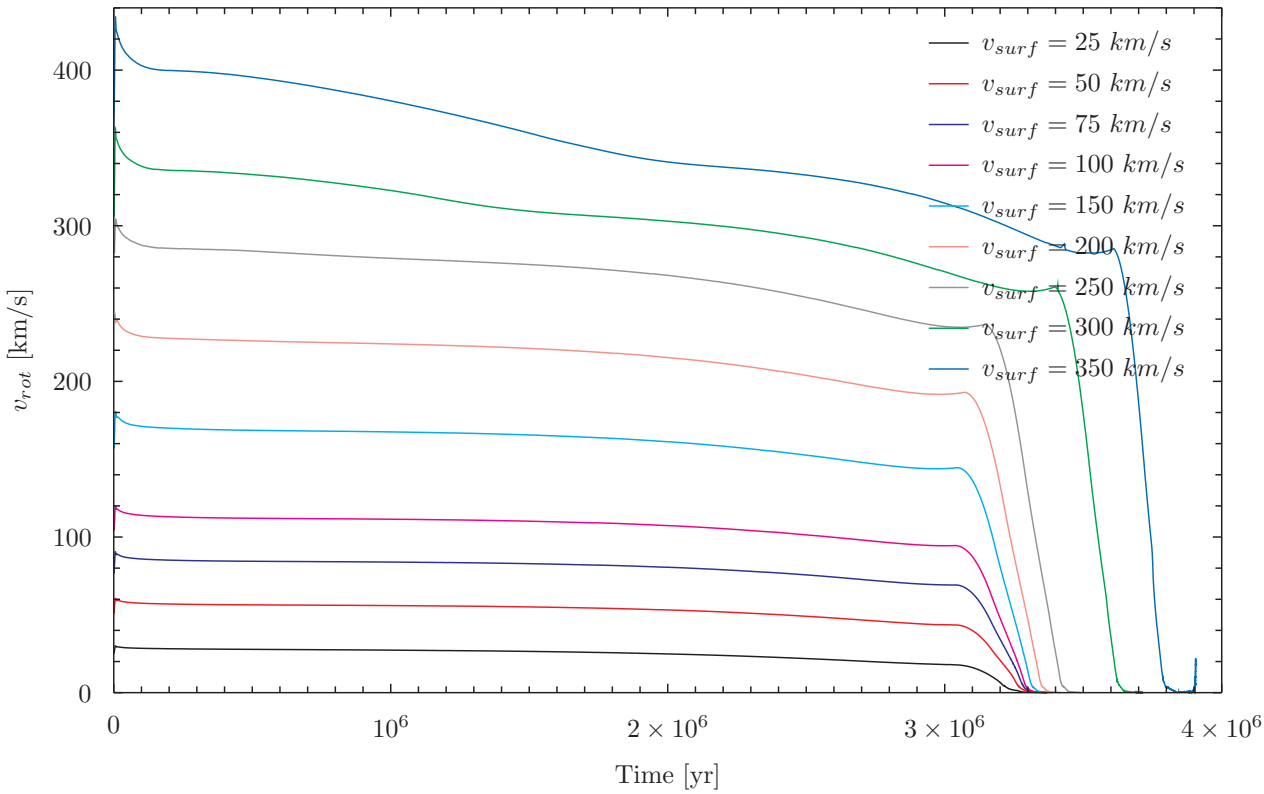

Fig. 3.12: The rotational velocity of the shell with the maximum Eddington factor as a function of time for $60M_\odot$ models. A quick spin down of the shell (and therefore, star as rigid body rotation is assumed) occurs when mass is lost. The small spikes in velocity represent a change in the location of the maximum Eddington factor in the star. In general loss of angular momentum due to mass loss causes the star to spin down.

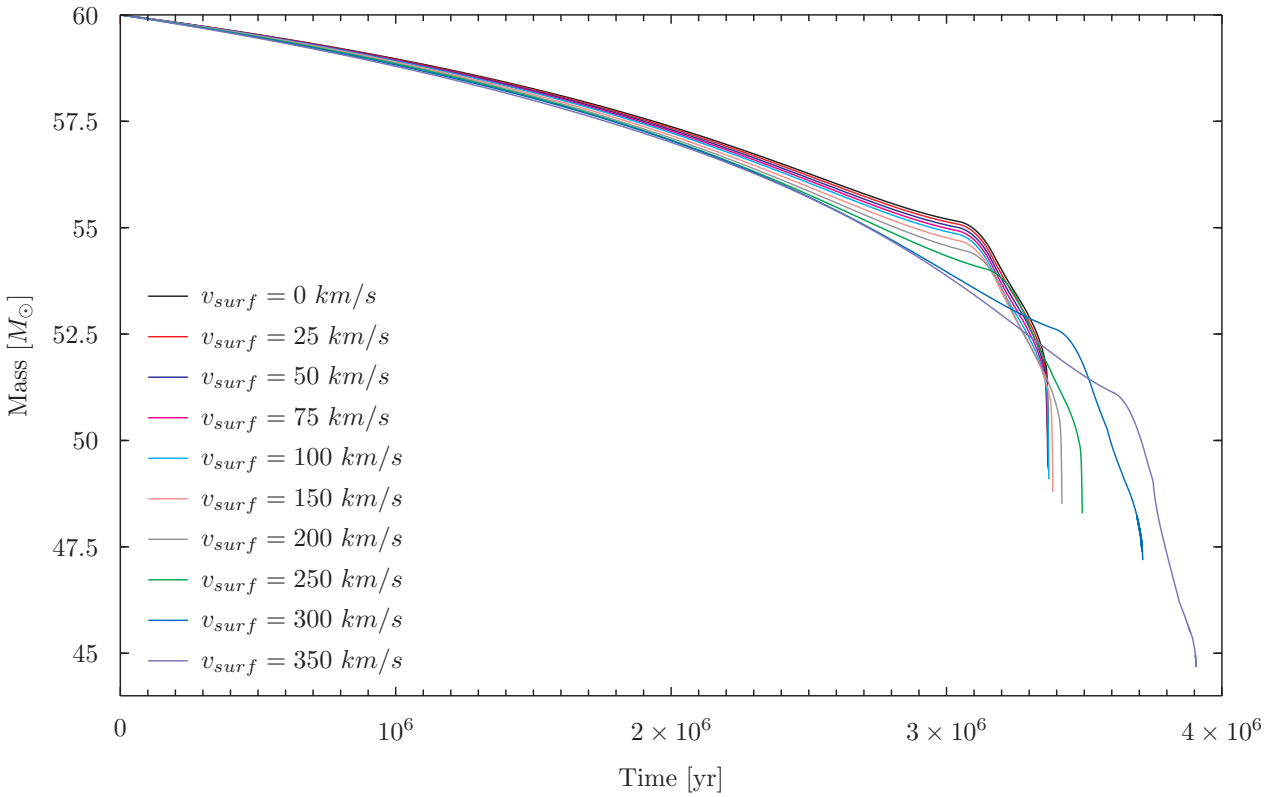

Fig. 3.13: The mass of $60M_\odot$ models as a function of time. All of them have a mass of approximately 50 $M_\odot$ at the end of the main sequence.

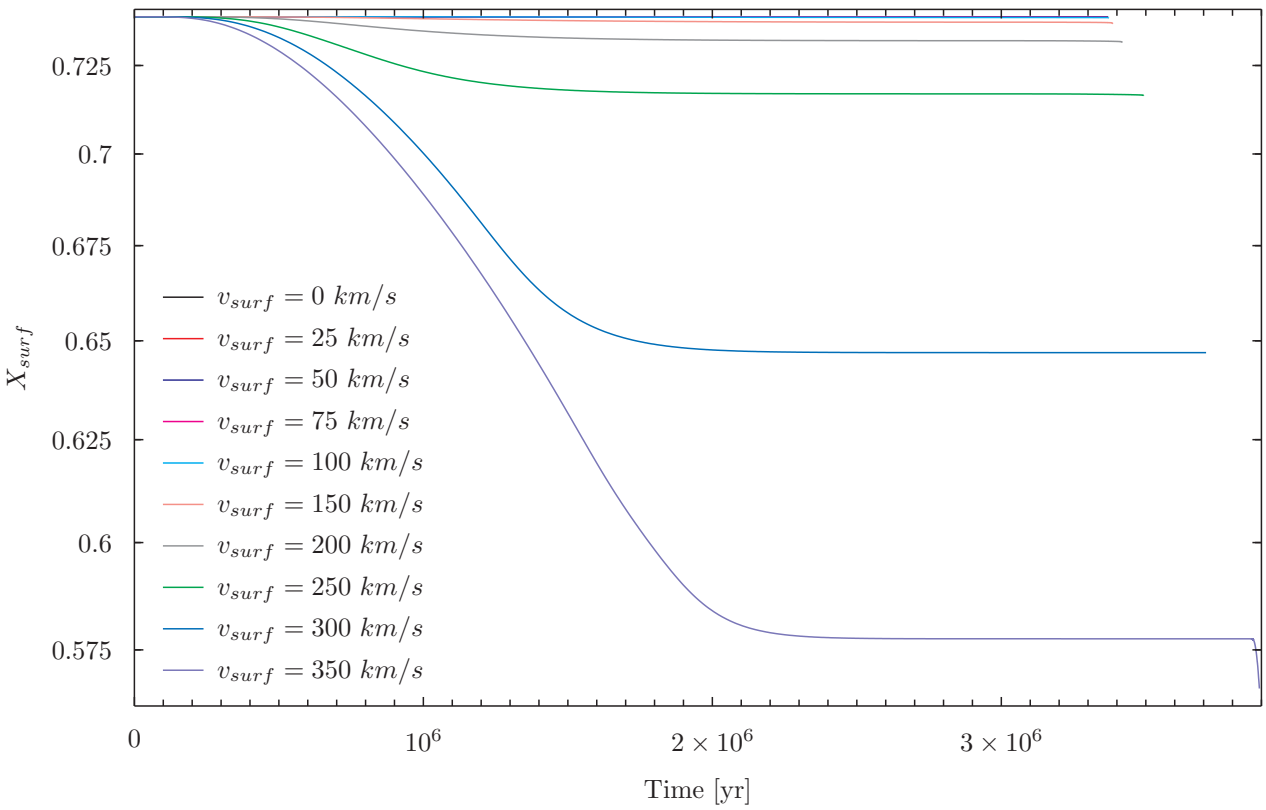

Fig. 3.14: The surface abundance of hydrogen as a function of time for $60M_\odot$ models. Significant hydrogen depletion during the main sequence is only achieved for the fastest rotating model.

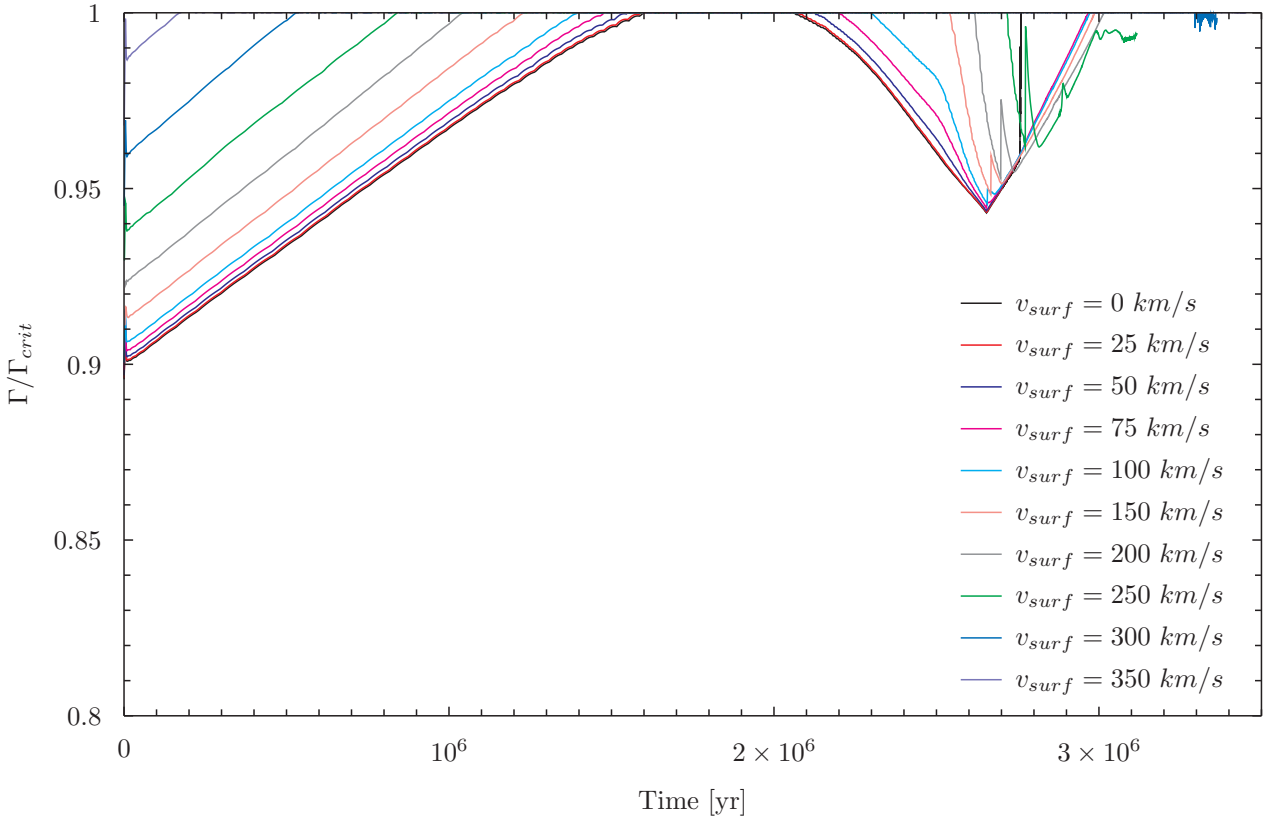

Fig. 3.15: The relative eddington factor as a function of time for $80M_\odot$ models.

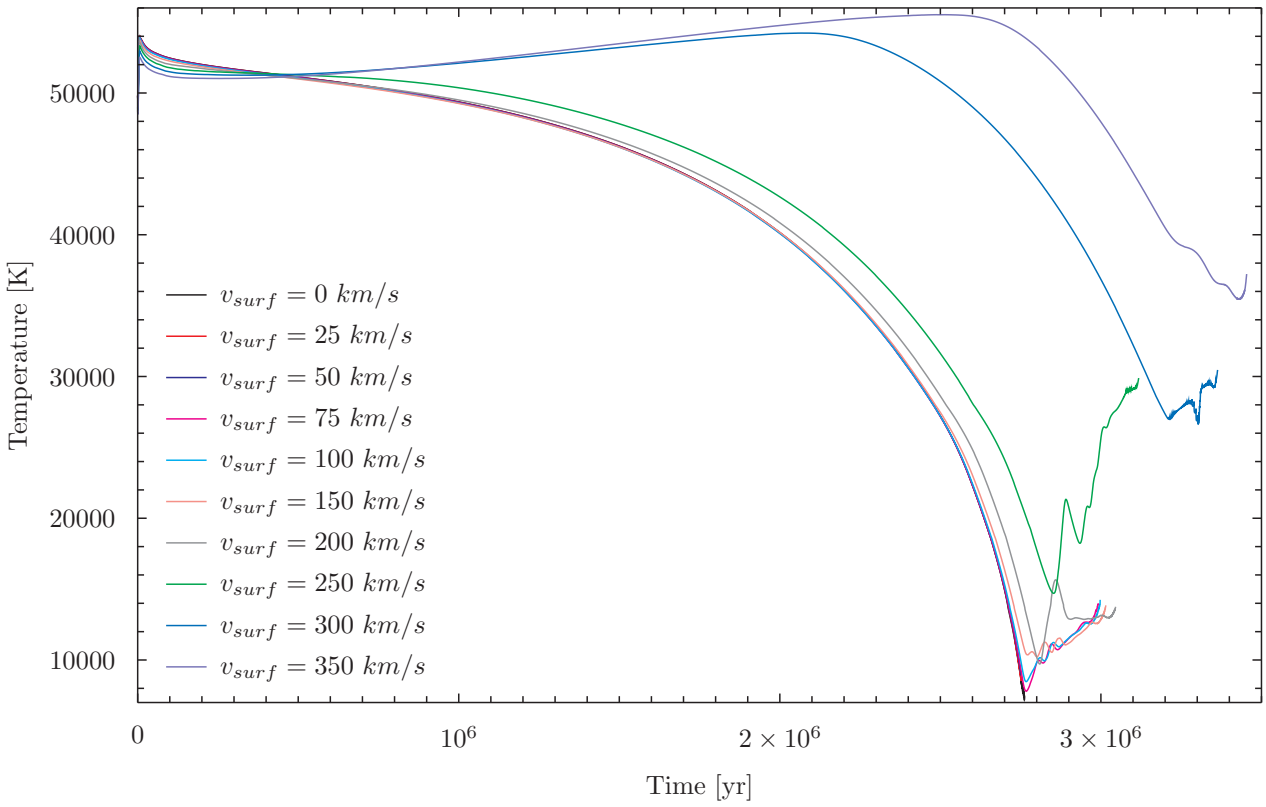

Fig. 3.16: The surface temperature as a function of time for $80M_\odot$ models.

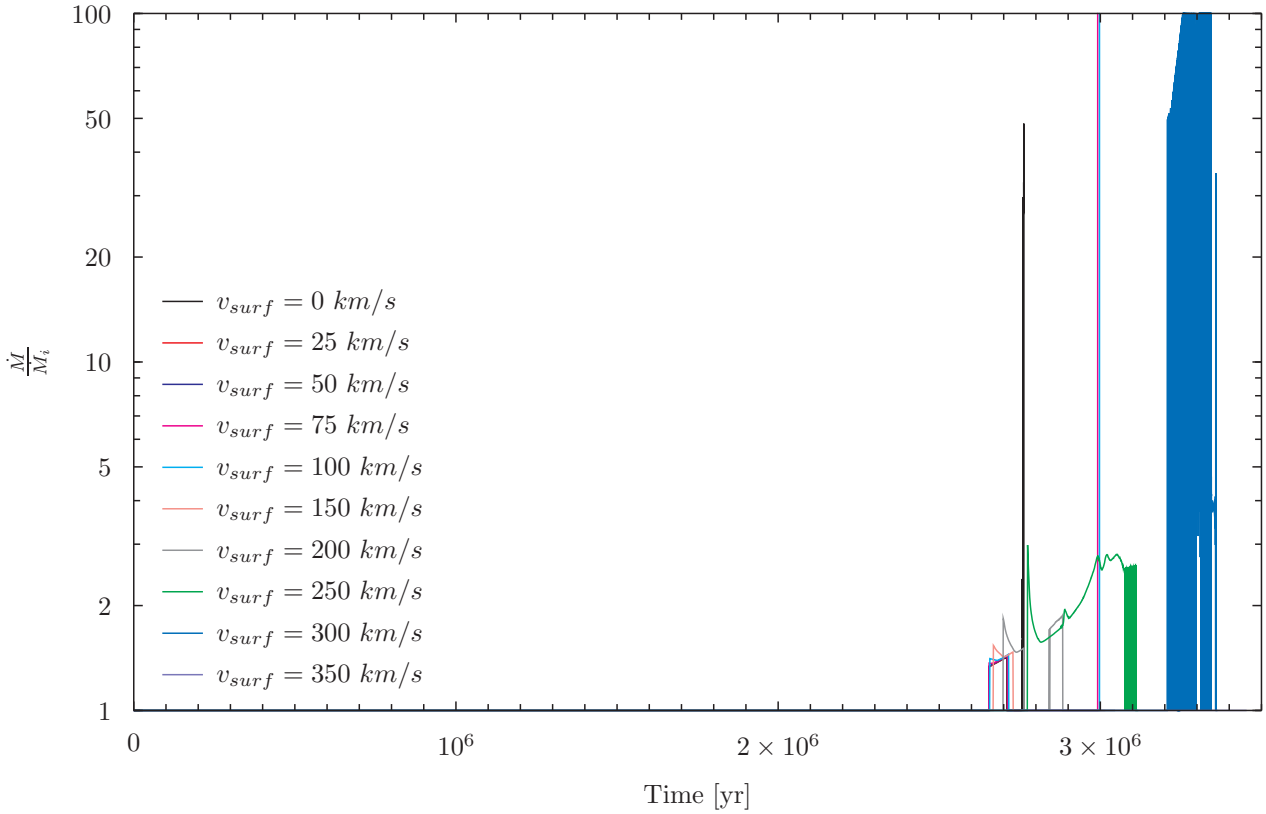

Fig. 3.17: The relative mass loss rate as a function of time for $80M_\odot$ models.

in their main sequence evolution than $60M_\odot$ models so they have more hydrogen in their core when Eddington mass loss occurs. In Figure 3.16, we observe that the effect of rotation on the star and on Eddington mass loss is quite noticeable. Rotation causes the stars to turn bluewards at hotter temperatures (earlier) because of the increased Eddington mass loss due to both the longer periods of mass loss (lower $\dot{T_{eff}}$) and the larger mass loss rates (Figure 3.17).
An interesting feature that was not visible in the $60M_\odot$ models is the variability in the surface temperature after mass loss occurs. All models gradually move bluewards but there are phases in their evolution where they may switch direction and move redwards. The model initially rotating at $v_{surf} = 200\ km/s$ moves redwards for around 150,000 years soon after Eddington mass loss has subsided. The $v_{surf} = 250\ km/s$ model has a briedisappearf period of redward movement while Eddington mass loss is still in progress approximately between 2.96 and 2.97 million years. These features are similar to LBVs which move across the Humphreys-Davidson limit over a number of years but they are not as impressive or as fast as LBV transitions.

Due to the fact that these models arrive at the Humphreys-Davidson limit much earlier in their evolution (the non rotating model still has 13% hydrogen in its core), they have time to deplete the hydrogen at the surface of the star before core collapse (Figure 3.18). At the end of the main sequence, these stars have a surface hydrogen abundance of $X = 0.32$ which means that they are probably WNL stars unlike the $60M_\odot$ models which may still be classified as Of stars. The fastest rotators have lost over 30% of their mass to stellar winds which will have a significant impact on their post main sequence evolution. It must be noted that the core and envelope mass do not decrease by the same proportion. The Kippenhahn diagram of a model initially rotating at $v_{surf} = 250\ km/s$ (Figure 3.19) shows the distinction clearly. Before the bi-stability jump the mass loss rate is low and the core and envelope mass loss are in sync. However, when the mass loss rate later increases, the timescale is short enough that the envelope decreases much more than the core.
We now know that the Eddington mass loss prescription affects the turning point of these models. For the $60M_\odot$ models, we saw that the mass loss does not keep stars away from the Eddington limit as we originally assumed. In these models, we observe a similar trend. As Figure 3.15 highlights, the increased mass loss again moves the star closer to the Eddington limit. However, for the fastest rotators, we that stars reach a limiting Eddington factor while mass loss occurs and evolve parallel to the Eddington limit. This trend is much clearer in the $100M_\odot$ models so it is discussed in more detail in the next section.

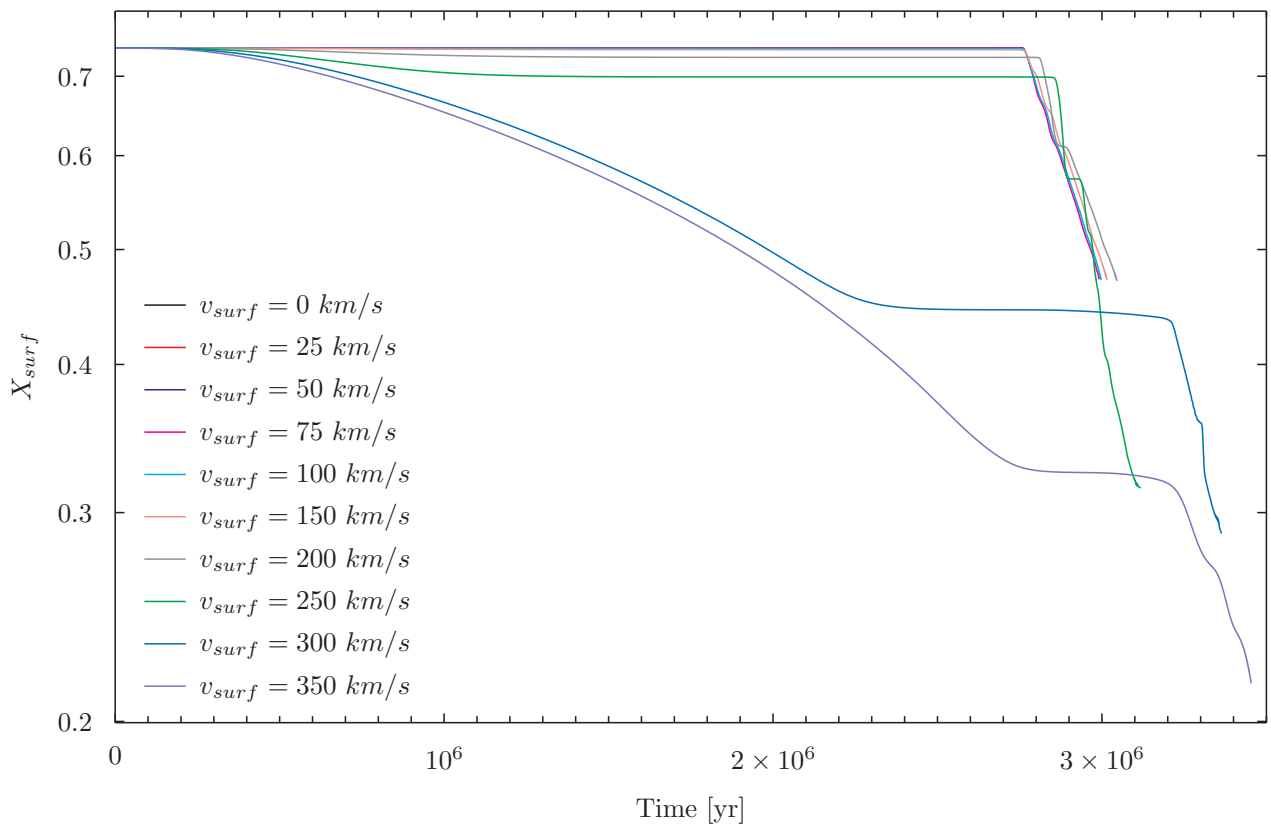

Fig. 3.18: The surface hydrogen abundance as a function of time for $80M_\odot$ models. These stars have hydrogen abundances in the ranges of observed WNL stars.

3.3 $100M_\odot$ models

The $100M_\odot$ models express the trends seen in the $60M_\odot$ and $80M_\odot$ models more plainly. The period of Eddington mass loss is extended further than for either the $60M_\odot$ or $80M_\odot$ models (Figure 3.20, 3.21) the mass loss is also more intensive leading to a situation where all models turn bluewards very soon after Eddington mass loss is initiated. Similar to the fast rotating $80M_\odot$ models and unlike the others, the intense mass loss prevents the formation of a Hydrogen convection zone near the surface as the stars do not reach a cool enough temperature. After the Helium convection zone is created, the location of the maximum Eddington factor is at a depth shallower than τ_{max} and while the star initially does move to slightly cooler temperatures (as inferred by the increasing τ in Figure 3.22), mass loss quickly halts its cooling and the star turns bluewards. This is visible in all of the $100M_\odot$ stellar models.

A plot of the Eddington factor as a function of time (Figure 3.23) shows a clear trend - these models evolve almost parallel to the Eddington limit while Eddington mass loss is occurring. This is likely due to the reduction of the radiative envelope relative to the convective core which leads to a reduced radiative luminosity and as $\Gamma \propto L_{rad}$, the star is kept away from the the Eddington limit. The relative reduction of the radiative envelope is only evident when rapid and sustained mass loss occurs which may explain why lower mass and slower rotating models do not show trend, which is the only evidence for the Eddington mass loss prescription keeping stars simultaneously away from the Eddington limit **and** the Humphrey-Davidson limit.

3.4 Varying τ_{max}

To constrain our mass loss prescription further, we increased τ_{max} to a value of 80 and ran a course grid of models with the same range of masses as before albeit with just four initial velocities ranging from 0 km/s to 300 km/s. Increasing τ_{max} produces several non-linear effects. As expected, for the slower rotating models with $v_{surf} < 300km/s$, the periods of Eddington mass loss were increased by a small fraction since the maximum Eddington factor is allowed to drive mass loss from a deeper location in the star. If the relationship between mass loss and the Humphreys-Davidson limit was linear, then a trend between the coolest temperature that the models reach and τ_{max} would be observed. In Figure 3.25,

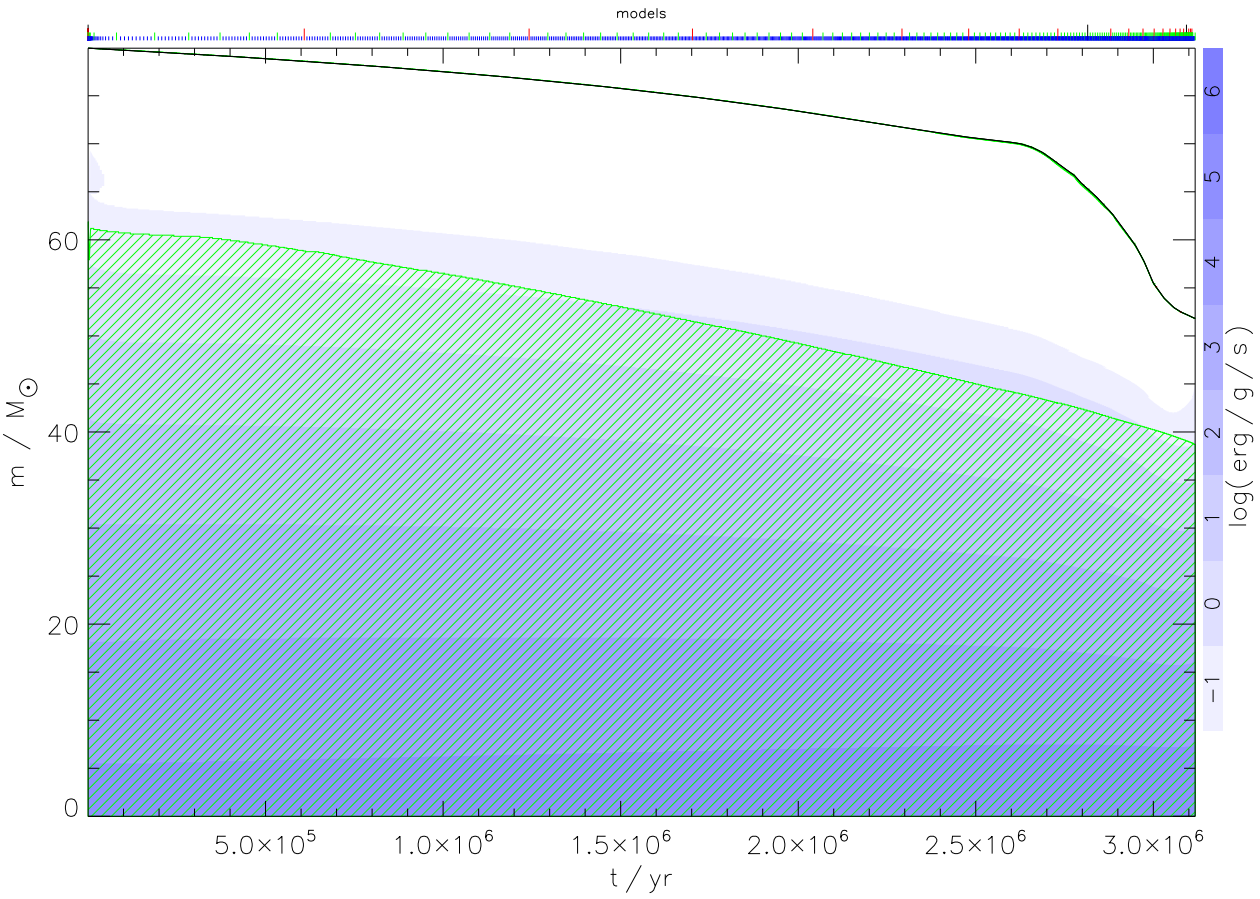

Fig. 3.19: The Kippenhahn diagram of an $80M_{\odot}$ star rotating initially at 250 km/s. We see several stages of mass loss in the diagram. Initially, the mass of the core and envelope reduce in sync but after the bi-stability jump, the envelope shrinks relative to the core.

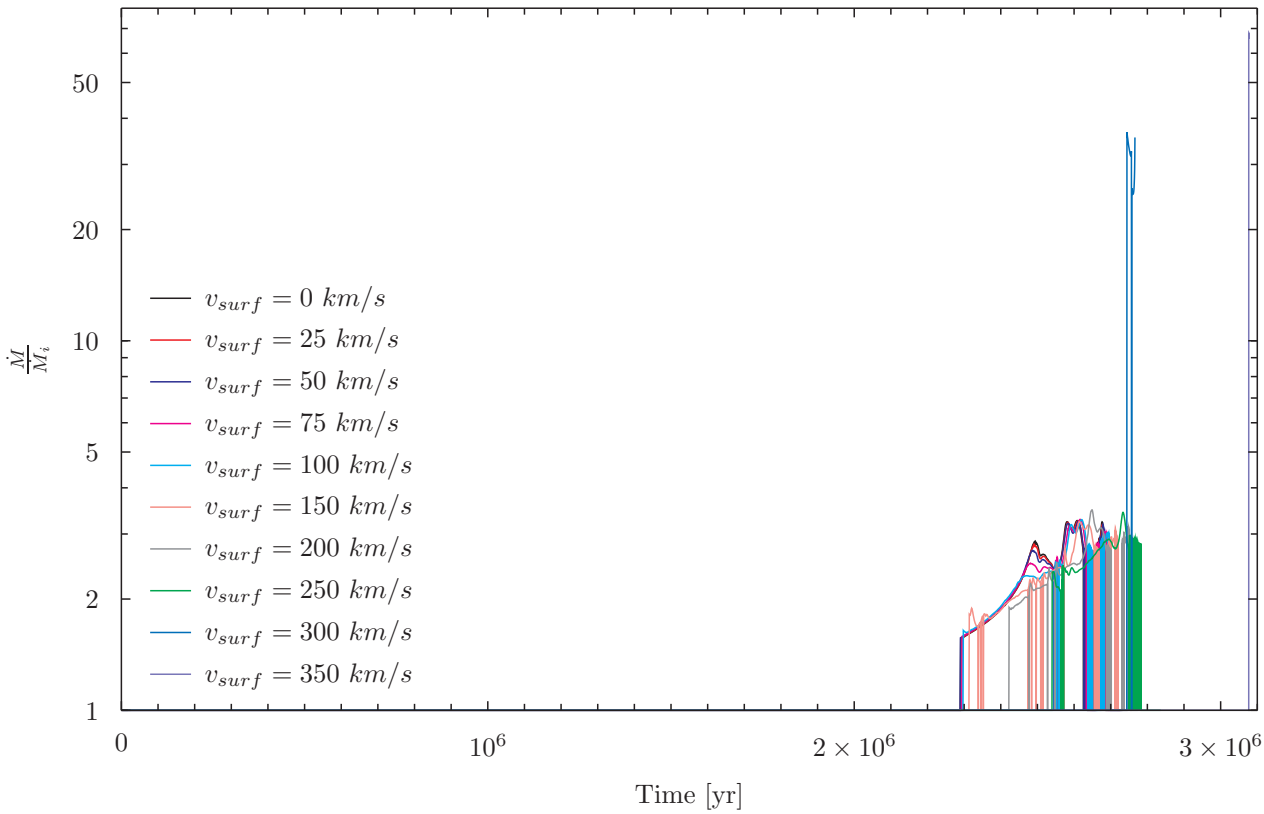

Fig. 3.20: The relative mass loss rate as a function of time for $100M_\odot$ models.

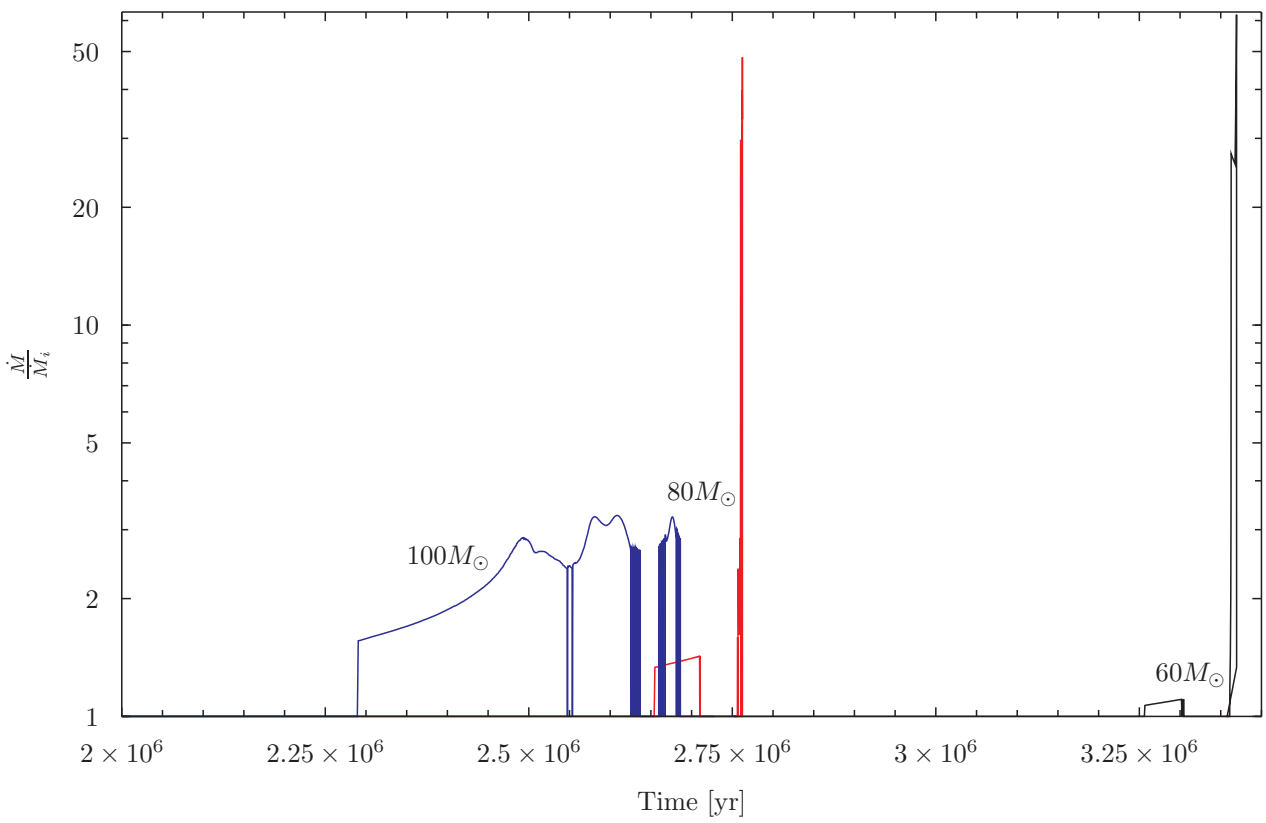

Fig. 3.21: The relative mass loss rate of the $60, 80$ and $100M_\odot$ non rotating models as a function of time. With increasing mass, the period and rate of mass loss increase.

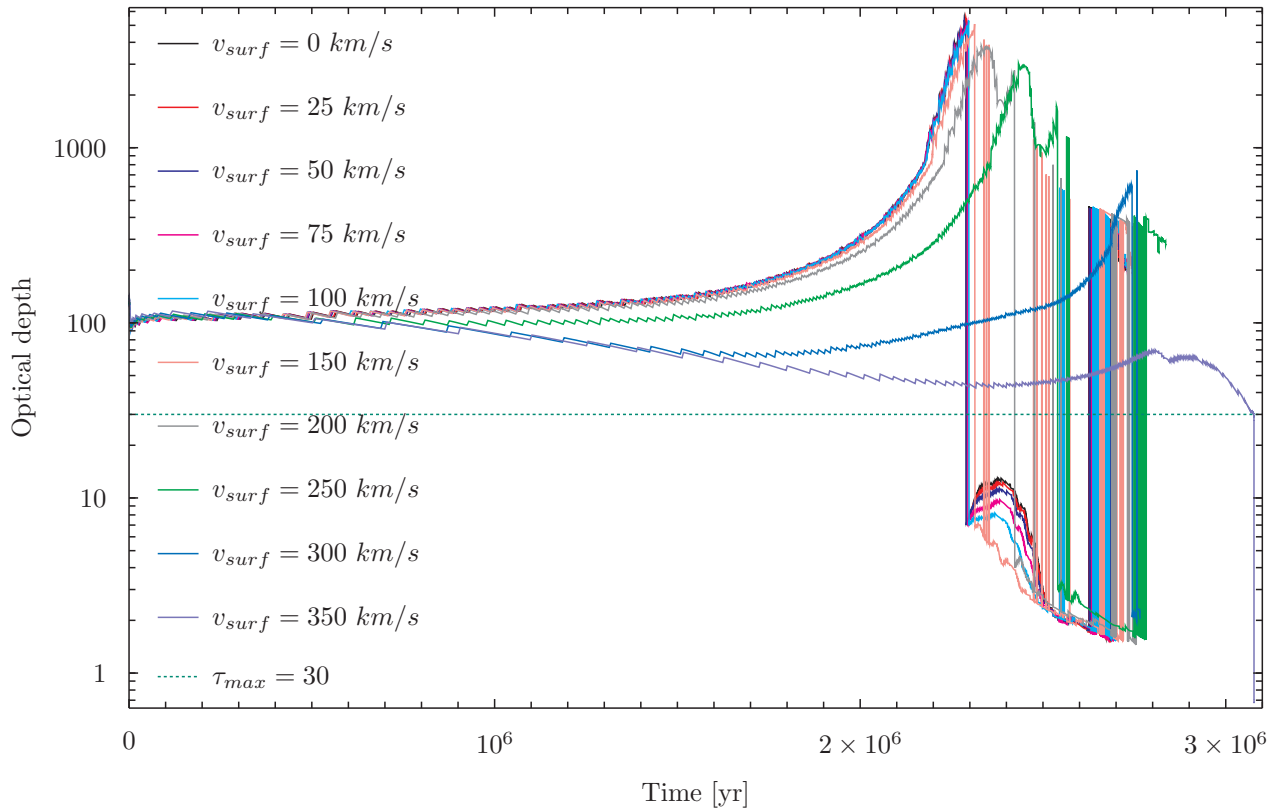

Fig. 3.22: The optical depth of the maximum Eddington factor as a function of time for $100 M_\odot$ models.

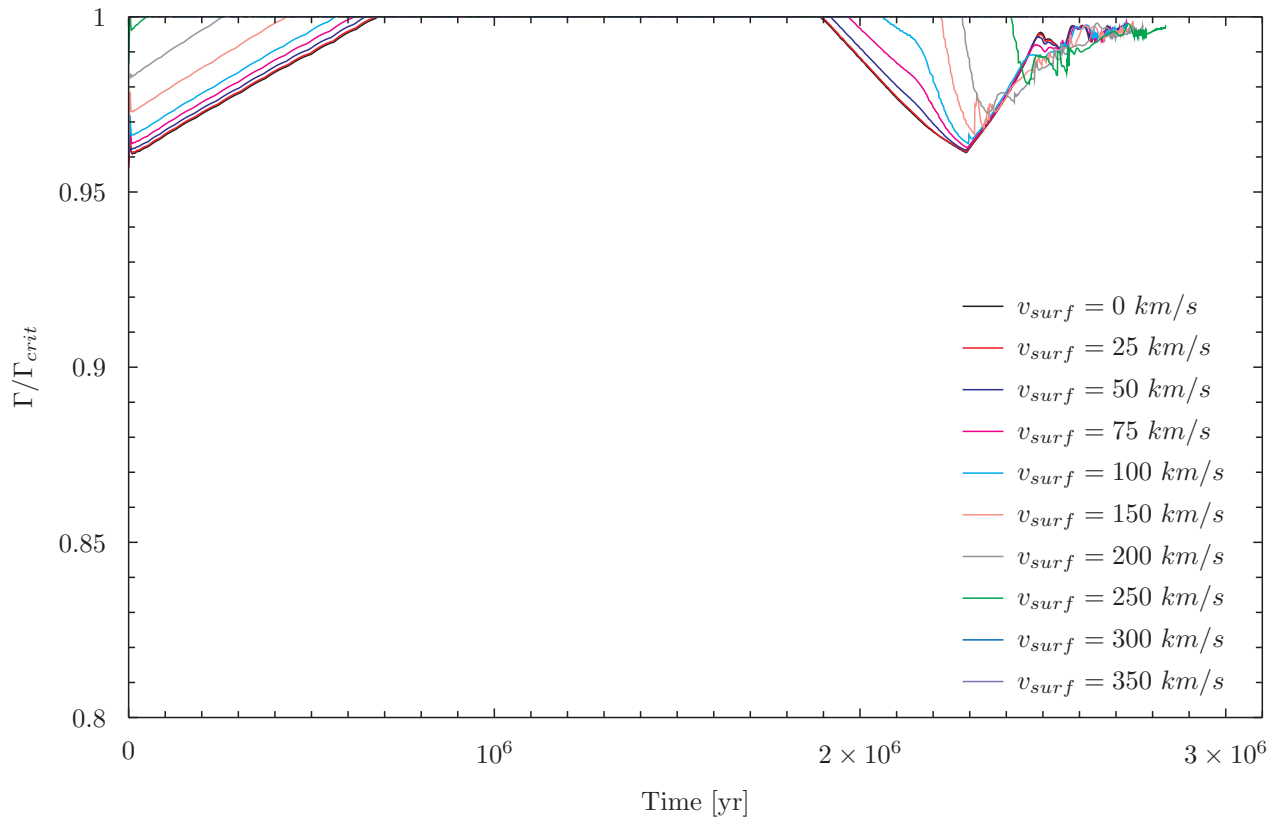

Fig. 3.23: The relative eddington factor as a function of time for $100 M_\odot$ models. The faster rotating models are closer to the Eddington limit.

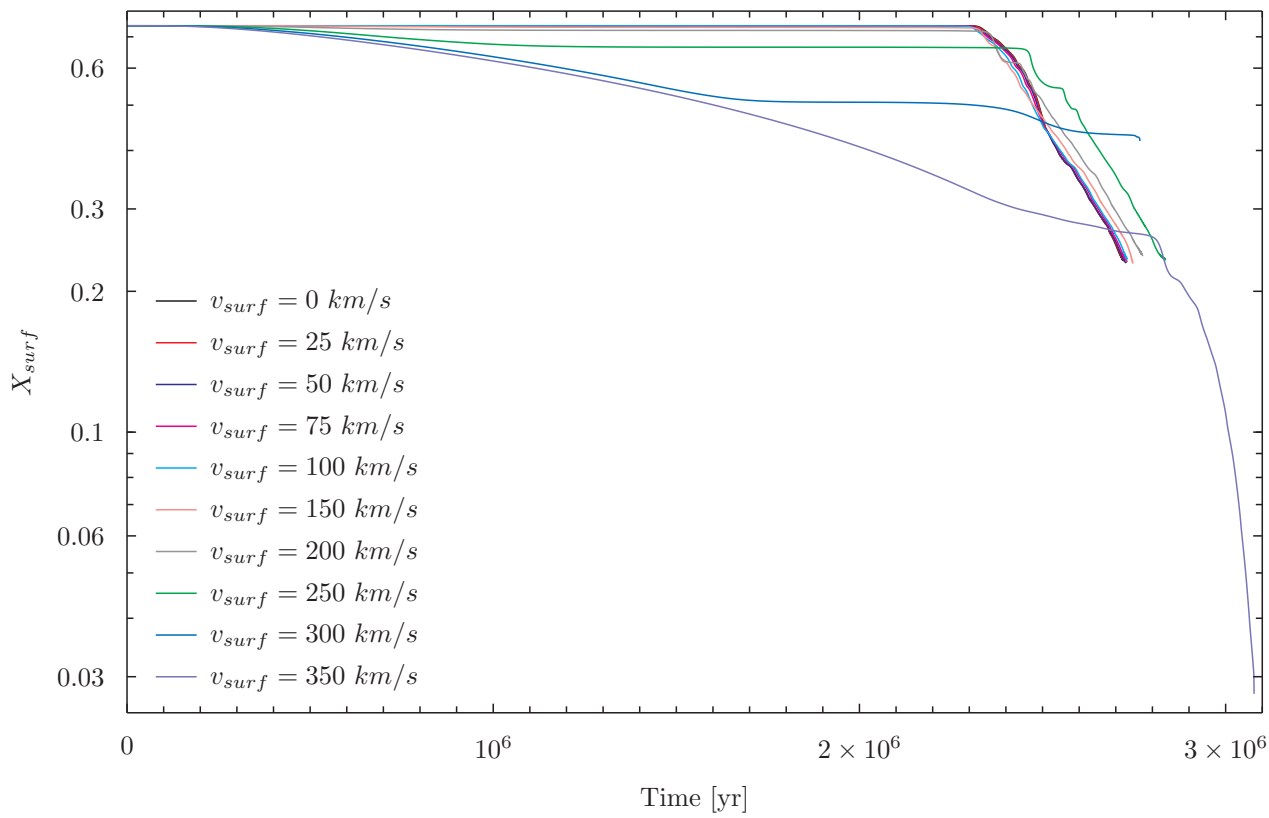

Fig. 3.24: The surface hydrogen abundance as a function of time for $100M_\odot$ models.

the coolest point in a model's evolution is plotted against its initial velocity for the two values of τ_{max} that we have calculated. The difference between the two sets of models is unclear. The turning points of the $60M_\odot$ and $100M_\odot$ models are barely affected by the increased τ_{max} while the $80M_\odot$ shows a small and fairly insignificant increase in the average turning temperature.

We note that both the $80M_\odot$ and $100M_\odot$ 300 km/s models actually have a cooler turning point which is due to Eddington mass loss occurring while the Fe convection zone is near the surface. In Figure 3.26, the optical depth of the maximum Eddington factor is plotted against time. Eddington mass loss occurs when τ is smaller than τ_{max} so mass loss occurs early in the evolution of these stars. Due to the models evolving in the proximity of τ_{max}, the mass loss is intermittent (Figure 3.27) (although less intermittent than suggested by the graph due to numerical damping present in our code; results are unaffected) which is most likely unrealistic as there have not been observations of intermittent mass loss in that region of the H-R diagram. Instead, scaling the mass loss with τ may be more accurate. The effect of this early mass loss on the star is visible in the evolutionary tracks of these stars in the H-R diagram (Figure 3.28) which, after partially chemically homogeneous evolution, turn bluewards and sharply decrease in luminosity. They then resume their redwards evolution with tracks similar to slower rotating models. They do not cross the Humphreys-Davidson limit during their main sequence evolution so this is acceptable behaviour from that point of view. On the other hand, there have been no definitive observations of young stars that have lost close to 30% of their mass. However, the dense shell of mass around them may disguise hot, young stars as older, less massive ones.

Future hydrodynamic wind modelling studies may identify a specific value of τ_{max} or alternatively, they might find that it varies with other physical parameters and is not as simple as our models. Current studies by Vink et al.; Gräfener et al. do not consider a stratified stellar structure or a peak in the Eddington factor below the surface of the star and are therefore not very useful for our work. Observationally, τ_{max} may also be constrained by correlating observations of young, luminous stars with high mass loss rates (eg. $-5.30 < log(\dot{M}[M_\odot/yr]) < -3.30$ for $100M_\odot$) with a population synthesis study. If a large number of young stars with high mass loss rates are found, then τ_{max} may be a large value. Conversely, if no young stars are observed with these features, τ_{max} may need to be closer to our original value of 30.

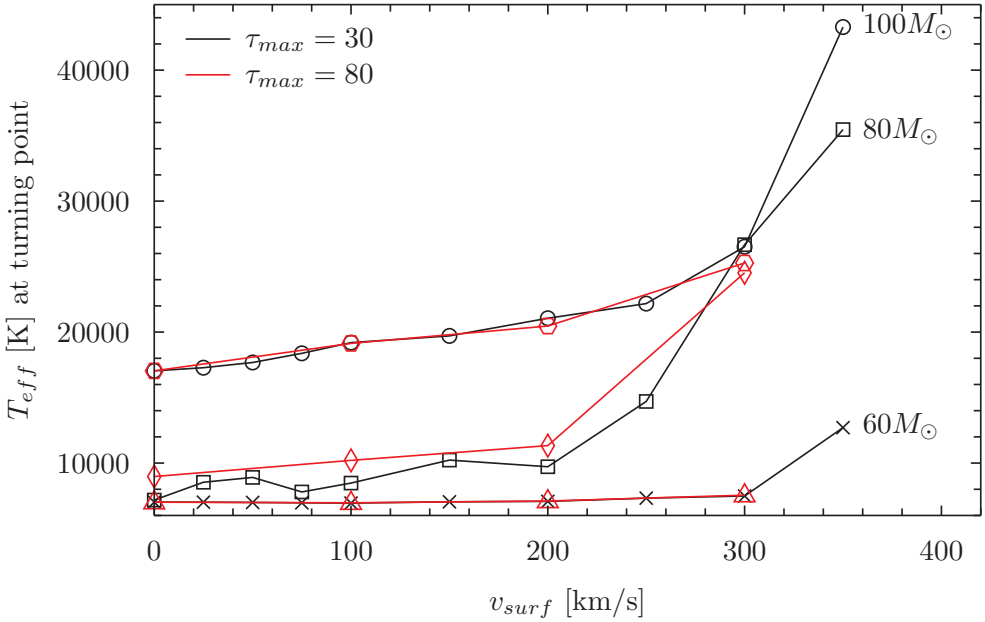

Fig. 3.25: The coolest temperature in the evolutionary track is plotted against the initial surface velocity for the two values of τ_{max}. We do not see a particularly clear trend between the sets of simulations but in general, the higher τ_{max} forces the star to run bluewards at hotter temperatures. The mass dependence of this effect is unclear as it appears to more strongly affect the $80M_\odot$ models than either the $60M_\odot$ or the $100M_\odot$ models.

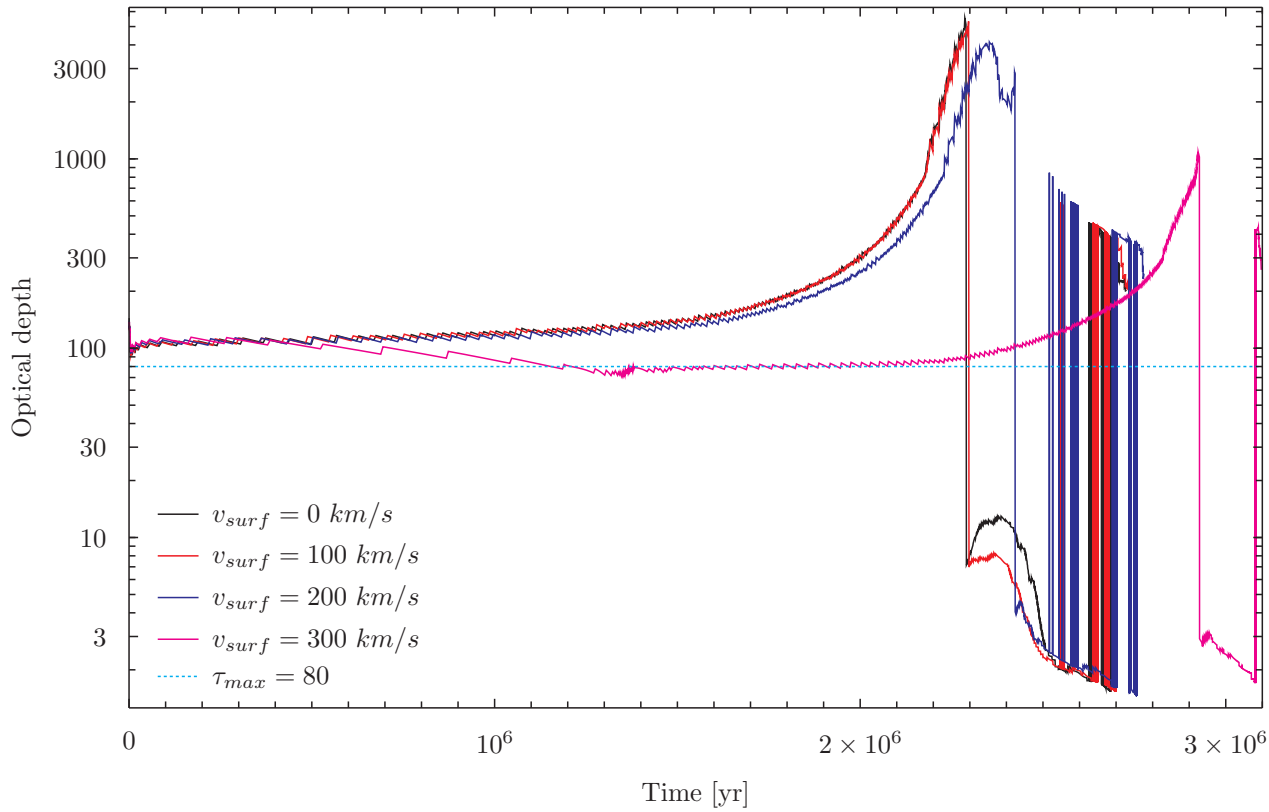

Fig. 3.26: The optical depth of the maximum Eddington factor as a function of time for $100M_\odot$ models. The maximum Eddington factor in the $v_{surf} = 300\ km/s$ model dips below $\tau = 80$ while the iron convection zone is near the surface. This drives Eddington mass loss earlier than in other models. The same phenomenon occurs in the $80M_\odot$ model fast rotating model.

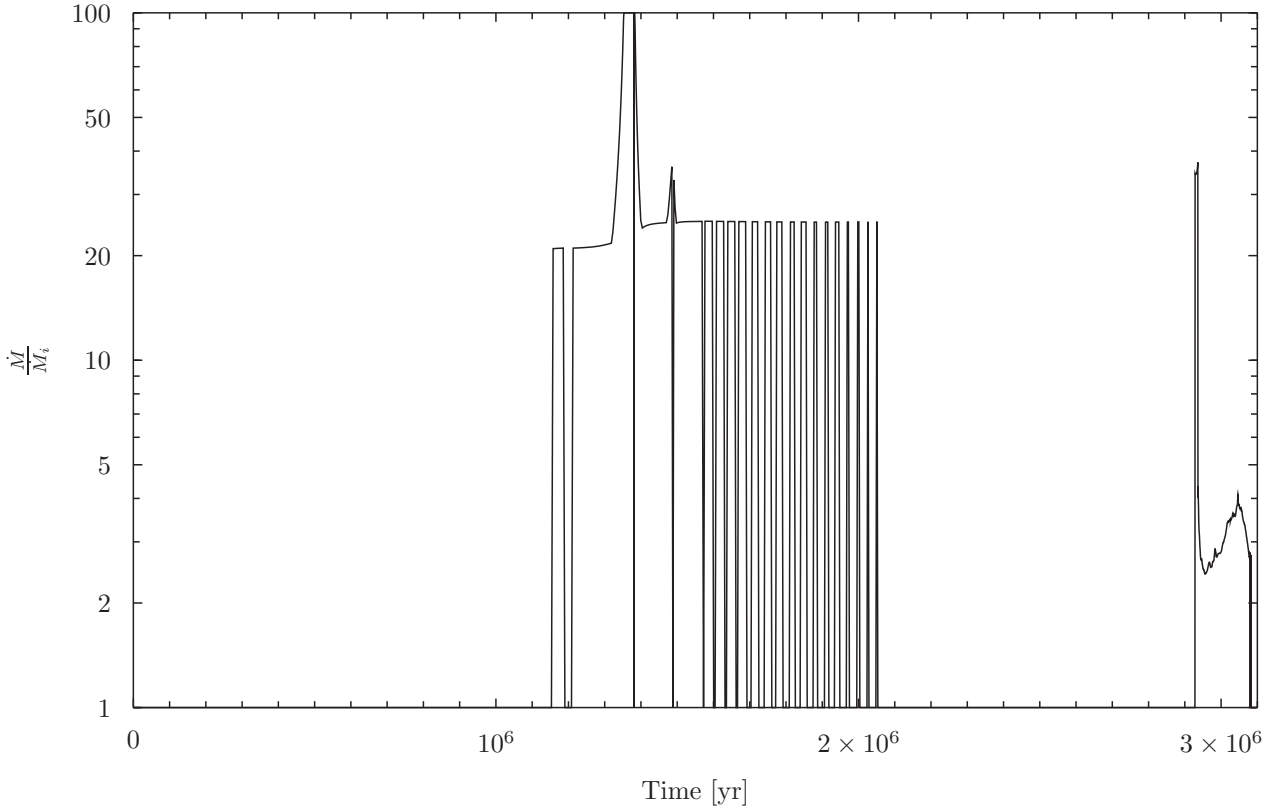

Fig. 3.27: Mass loss of the $100M_\odot$ model rotating initially at 300 km/s is intermittent because it evolves close to the optical depth criteria. Our code dampens the intermittence of the mass loss rate by averaging it over a number of models so that it does not change so dramatically but this is not depicted in the graph. Its effect is minimal.

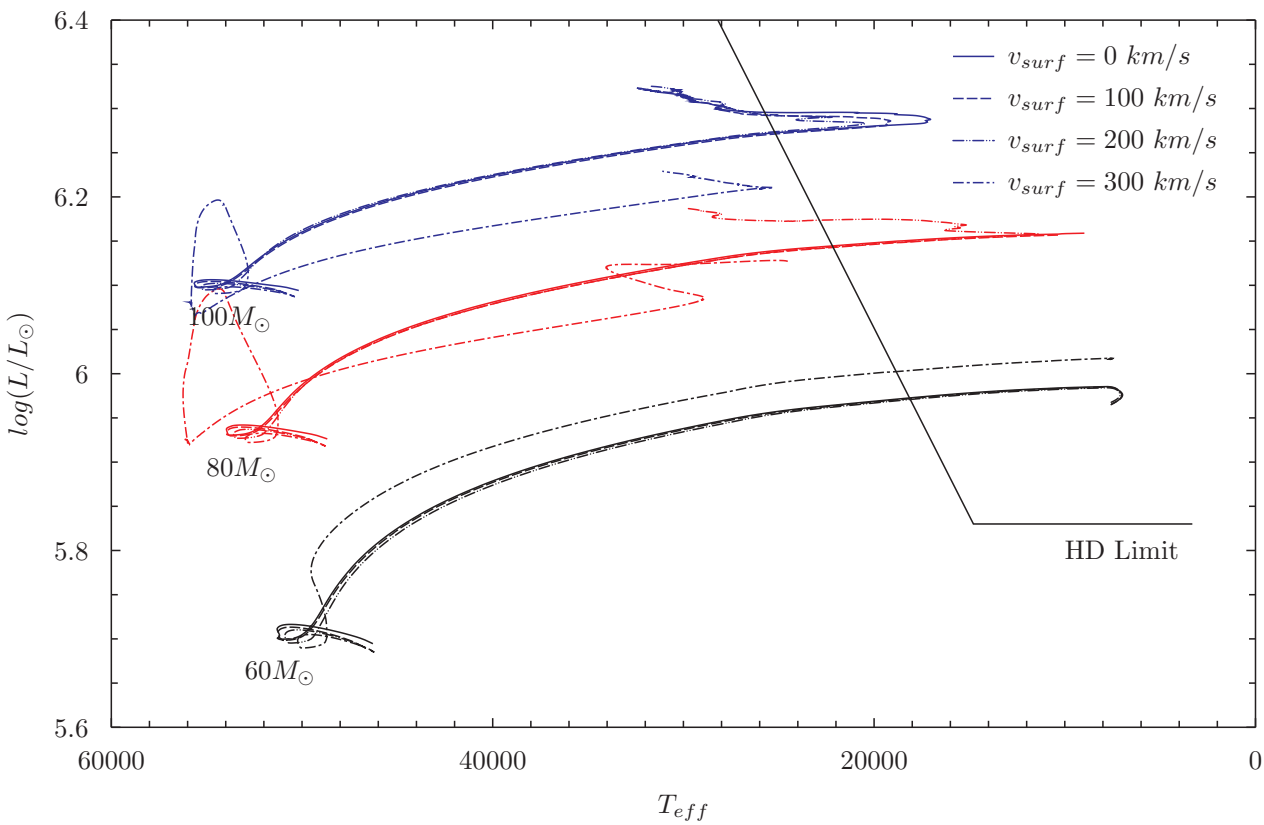

Fig. 3.28: A Hertzsprung-Russell diagram plotting models simulated with $\tau_{max} = 80$. The main difference between this and Figure 2.4 at $\tau_{max} = 30$ is effect of Eddington mass loss on the fast rotating models early in their evolution.

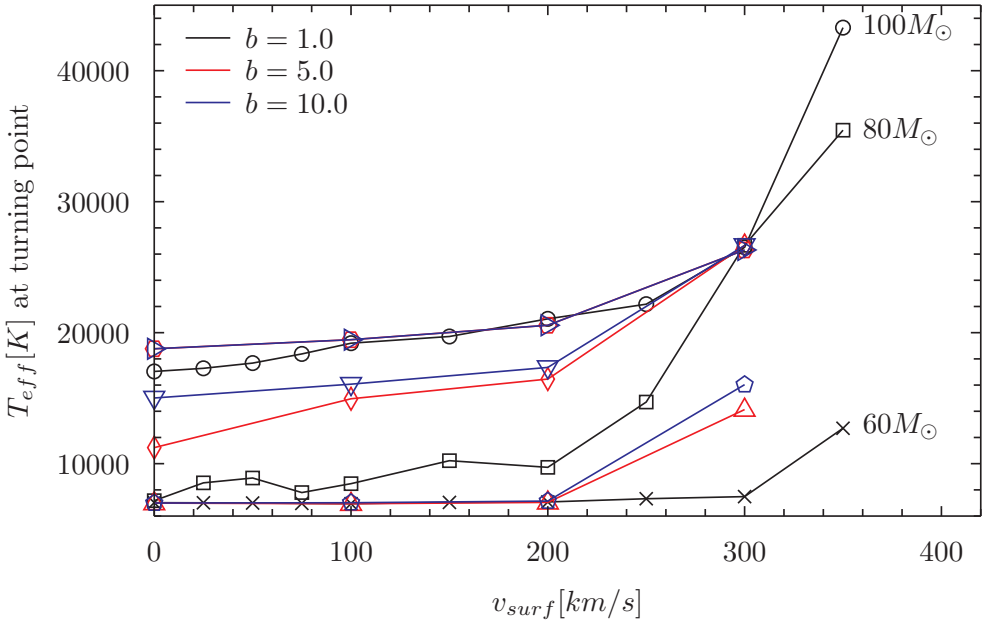

Fig. 3.29: The coolest temperature in the evolutionary track is plotted against the initial surface velocity for the three values of b. Increasing b means that stars generally turn at hotter effective temperatures. Similarly to varying τ_{max}, this effect is significant in faster rotators and higher mass models (especially $80M_\odot$) while only modestly modifying the evolution of the $60M_\odot$ models. Larger values of b show increasingly weaker improvements.

3.5 Varying b

Larger values of the mass loss parameter b were considered. b is analogous to the wind efficiency parameter η (Vink et al. 2000) and larger values of b imply a stronger driving of the wind. The course grid in Section 3.4 was used to calculate models with $b = 5, 10$. We reverted back to $\tau_{max} = 30$.

Figure 3.29 highlights the effect of larger values of b on the evolution of the star. The turning point temperature increases on average and this is most evident in the $80M_\odot$ models, just as with τ_{max}. However, larger values of b only produce marginal increases in the turning point temperature. The ineffectiveness of the increased mass loss rate on the $60M_\odot$ models can be attributed to the lateness of Eddington mass loss. Near the end of the main sequence, the rate of core contraction (and envelope expansion) increases. This means that a disproportionately greater mass loss is required to turn the star bluewards quickly which is not present in our mass loss prescription. Furthermore, the slow rotating $60M_odot$ stars do not have a sufficiently strong gradient in mean molecular mass and subsequently, small amounts of mass loss does not sufficiently increase the surface temperature of the star. This is clearly demonstrated when the surface hydrogen abundances of $60, 80$ and $100M_\odot$ models are compared (Figures 3.14, 3.18, 3.24).

Chapter 4

Conclusions

4.1 Summary

We have presented a new mass loss prescription for luminous stars by building upon the work of Vink et al. (2000), Nieuwenhuijzen & de Jager (1990) and Hamann et al. (1995) and adding a Γ dependence on the mass loss. We then calculated stellar evolution models of stars of $60, 80$ **and** $100 M_{\odot}$ masses initially rotating at velocities ranging from $0 - 350\ km/s$. We also varied free parameters b and τ_{max} in the mass loss prescription and identified their importance, finding that changes to τ_{max} affects evolutionary tracks of the 80 and $100 M_{\odot}$ stars significantly and also non-linearly. This complicates the calibration of these parameters with observations.

We did not attempt to parametrize the α parameter which changes the gradient of the Γ-$\frac{\dot{M}}{\dot{M}_i}$ law or Γ_{min}, settling with sensible defaults. Vink et al. (2011) find a strong kink in the classical Eddington factor, Γ_e, dependence of $\dot{M}$, which is $\dot{M} \propto \Gamma_e^{0.7}$ for "low" Γ_e but rises to $\dot{M} \propto \Gamma_e^{3.99}$ for the "high" Γ_e regime. Since we only model a smooth, gradual increase of $M(\Gamma)$ (eg. Figure 2.1, this kink may influence our results. They only consider the classical Eddington factor so the location or properties of this kink may differ when the full Eddington factor, Γ is considered with the opacities of all spectral lines.

Compared to mass loss measurements of massive stars in the LMC by the VLT FLAMES survey (Mokiem et al. 2007b), our values are generally on the higher side. The majority of observations are however of less luminous stars and there are few measurements of stars near the Humphreys-Davidson where our mass loss rate predictions ($10^{-4} M_{\odot}/yr$) (Figure A.2) are a magnitude or so larger than measurements. However, there are uncertainties due to clumpiness and other factors which may increase or decrease the measured mass loss rates. Furthermore, the surface hydrogen abundance Of and WNL models in the HR diagram generally match observations by Evans et al. (2010). We again emphasize that this study is qualitative rather than quantitative and a proper calibration of mass loss parameters are required.

Our mass loss criteria assumes that mass loss only occurs when the optical depth of the maximum Eddington factor is below a certain value (τ_{max}) and the transition between phases of Eddington mass loss and no Eddington mass loss is a sharp switch. This, however, may be too strict and we question the efficiency of the damping described in Section 2.1 to prevent Eddington mass loss, especially near the τ_{max} boundary where mass loss should ideally be scaled relative to the optical depth to create a smooth transition between phases of Eddington mass loss. The intermittent mass loss in Section 3.4 is unrealistic but Guzik et al. (2005) consider such effects in LBVs which occur on short timescales due to pulsations and a similar theory may be applied to this work. At certain points in the evolution of these models, super-Eddington luminosities existed at optical depths greater than τ_{max} and the stellar interior may not be as stable as we assumed. However, as our stellar evolution code did not complain about hydrodynamic effects at those points, our assumption may not be that far from the truth.

The results obtained with this mass loss prescription are promising and a step in the right direction. However, it does fail to account for the Humphreys-Davidson limit near the slow-rotating $60 M_{\odot}$ models. Increasing the optical depth criteria and scaling up the mass loss rate did not cause them to turn redwards at a hotter temperature and this is very discrepant with observations. A population synthesis study with an initial mass function and initial velocity function based on observations would clarify this better. On the basis of these results, however, it is safe to say that our prescription is missing some physics dealing with lower mass stars.

It is possible that our optical depth criteria is too simplistic - Pistinner & Eichler (1995) observe iron convection zones near the surface of Wolf-Rayet stars. Our models focus on O and Of stars but Eddington mass loss driven by iron convection zones rather than helium (the case for the vast majority of our models) may provide a solution to the $60 M_{\odot}$ discrepancy. Our initial investigation of mass loss driven by the iron convection zone produced "strange" results which were not supported by previous studies. The implementation of such mass loss would require a substantially different optical depth criteria, perhaps $\tau_{max} = \tau_{max}(M)$. Alternative optical depth criteria such as $\tau/R_{depth} < 1 \times 10^{-11}$ or $\tau/R_{depth}^2 < 5 \times 10^{-25}$ could instead be used. These criteria remove the possibility of iron convection zone driven mass loss but allow for an extended period of hydrogen convection zone driven mass loss which may turn $60 M_{\odot}$ stars bluewards quicker. These criteria may be justified on the basis that winds originating deeper in the star have the potential to destabilize more mass and therefore drive stronger mass loss.

Our work might modify the massive star evolution diagram from Langer (2012) (Figure 1.7) as high mass stars will appear as spectral type Of for a longer period of its main sequence lifetime (τ_{CHB}). In fact, 80 and $100M_\odot$ models are only considered to be WNL stars after Eddington mass loss occurs at around 75% of their main sequence evolution. For $60M_\odot$ models, it's even later than that. Stellar winds become optically thick at approximately $0.8\tau_{CHB}$.
Wind modelling studies by Vink et al. (2000, 2011) highlight the fact that the wind efficiency parameter η varies in time, depending on the opacity of the wind. At early stages of evolution, the wind is optically thin and η may be a low value close to 0.8. However, as the wind becomes optically thick, η increases to 3.0 and above (Vink et al. 2011), due to the multi-scattering of photons. This change drives a much denser wind and more disruptive mass loss. Our work may be affected by this feature because we assume that b, which is related to η, is constant during evolution. If b were to be modified by other physical parameters, we might see a weaker mass loss rate at earlier stages of evolution which might explain the discrepancy with large values of τ_{max} in Section 3.4.
The lack of recent work in this subject area makes it difficult to qualify the importance of our mass loss prescription. Langer (1998) studied the effect of the closely related Omega-limit for rotating stars assuming a $\dot{M}/\dot{M}_{(v_{rot}=0)} = (\frac{1}{1-\Omega})^\xi$ relation, with $\xi = 0.43$. However, no connection to the Humphreys-Davidson limit was made so the similarities to our investigation are limited. In that investigation, homogeneous conditions were assumed for optical depths less than 100 and the Eddington factor was calculated at some point within that region. However, our investigation considers the Eddington factor at a particular point, making use of the fact that opacity peaks exist near the surface which render the isotropicity condition invalid. Maeder & Meynet (2000) also focus on critical rotators and do not attempt to compare simulations to the Humphreys-Davidson limit.
In conclusion, we find that this mass loss prescription is a step forward in understanding the Humphreys-Davidson limit as well as the effect of the Eddington limit on the evolution of stars. It is therefore recommended for use in stellar evolution calculations once mass loss parameters have been calibrated with observational data. For sensible defaults, values of $\Gamma_{min} = 0.90$, $\alpha = 0.2$, $\tau_{max} = 30$, $b = 1.0$ are suggested as reasonable evolutionary tracks are achieved. While it does not address the $60M_\odot$ models well, it is still an overall improvement over previous theoretical mass loss prescriptions. Ideally, we would have liked to calculate models till the end of the helium main sequence and to consider WNE stars too but numerical difficulties prevented this. Future work may involve modifying the code to prevent these numerical problems but this is not an easy problem.

4.2 Future work

One important shortcoming of our mass loss prescription is that we have only considered the Eddington factor at a particular point in the star - where it is largest. It is likely that large Eddington factors do also exist at locations of lower optical depth and therefore drive Eddington mass loss earlier or more powerfully (due to the greater or lesser mass above the shell) than assumed in our models. Treating Eddington factors at multiple locations in the star will require a much more detailed treatment and may be consideration for future work.
Modelling the evolution of these stars using a combined stellar structure and atmosphere code such as Schaerer et al. (1996) could help greatly as this would model radiation driven winds occuring due to various subsurface convection zones. It would also consider the true Eddington factor at various positions under the stellar surface, unlike current wind models by Vink et al. (2011); Gräfener et al. (2011) and others. Combining this technique with a stellar evolution code to consider the Humphreys-Davidson limit as we do in our work would be a major advance in the field.
As mentioned previously, the free parameters τ_{max}, α, Γ_{min}, b and others could be calibrated with observations and hydrodynamic wind models. A population synthesis study would need to be carried out to fully appreciate the non-linearity of the parameters but comparing various properties such as luminosity, effective temperature, C/N ratio, hydrogen and helium abundances and other measureable quantities with observations of O, Of and WN stars would be a good way to constrain them. The upcoming VLT-FLAMES Tarantula Survey (VFTS) should provide us with the relevant data.
The modelling of heavier and lighter stars should also help to test the validity of this prescription. For stars more massive than about $200M_\odot$, the ZAMS curves to cooler effective temperatures Köhler & Langer (2012). There are very few observations of stars at these luminosities so we do not know how the Humphreys-Davidson limit fits into the scheme at those extremes. Those stars do not reach the low temperatures required for a Helium convection zone so if there is significant mass loss present (and observations suggest that there is), then it must either be driven by the iron convection zone or by other means. Stars that massive are usually at high redshifts and at low metallicities so they may not even have strong iron opacity peaks near their surface.
Sana & Evans (2011) found that the binary fraction for O stars is huge (in the galaxy), and between 45% and 75% of stars have spectroscopic companions. A large percentage are also in close binary systems so a precise binary code is required to model them. BEC is an optimal choice for this.
The mass loss prescription should be extended to other metallicities. Gräfener et al. (2011) find that "$\dot{M}(Z)$ relation for

WNL stars becomes flatter for higher Γ_e, i.e., high mass loss rates can also be maintained for very low Z.". This suggests that the relation between Eddington mass loss and metallicity is weak but it may not explain the evolutionary tracks of extremely high mass stars as mentioned previously.

Bibliography

Abbott, D. C. & Lucy, L. B. 1985, The Astrophysical Journal, 288, 679 12

Asplund, M., Grevesse, N., & Sauval, A. J. 2005, in Cosmic Abundances as Records of Stellar Evolution and Nucleosynthesis, Vol. 336, 25 20

Biermann, L. 1932, Zeitschrift für Astrophysik, 5 9

Bloecker, T. 1995, Astronomy and Astrophysics 7

Böhm-Vitense, E. 1958, Zeitschrift für Astrophysik, 46 9

Brott, I., de Mink, S. E., Cantiello, M., et al. 2011, Astronomy & Astrophysics, 530, A115 8, 9, 13, 14, 15, 17, 20, 29

Cantiello, M., Langer, N., Brott, I., et al. 2009, Astronomy and Astrophysics, 499, 279 3, 6

Canuto, V. M. & Dubovikov, M. 1998, The Astrophysical Journal, 493, 834 9

Chiosi, C. & Maeder, A. 1986, Annual Review of Astronomy and Astrophysics, 24, 329 12

De Loore, C., De Greve, J. P., & Lamers, H. J. G. L. M. 1977, Astronomy and Astrophysics, 61, 251 12

Endal, A. S. & Sofia, S. 1976, The Astrophysical Journal, 210, 184 9

Espinoza, P., Selman, F. J., & Melnick, J. 2009, Astronomy and Astrophysics, 501, 563 8

Evans, C., Hunter, I., Smartt, S., et al. 2010, The Messenger, 131, 25 8, 42

Evans, C. J., Taylor, W. D., Hénault-Brunet, V., et al. 2011, Astronomy & Astrophysics, 530, A108 8

Feldman, W. C., Asbridge, J. R., Bame, S. J., & Gosling, J. T. 1977, The Solar Output and its Variation 7

Fliegner, J. 1993, PhD thesis 8

Glatzel, W. 1994, Monthly Notices of the Royal Astronomical Society 14

Gräfener, G., Vink, J., de Koter, A., & Langer, N. 2011, Astronomy & Astrophysics, 1 8, 13, 15, 17, 38, 43

Grevesse, N., Noels, A., & Sauval, A. J. 1996, in Cosmic Abundances, Vol. 99, 117 20

Guzik, J. A., Cox, A. N., & Despain, K. M. 2005, The Fate of the Most Massive Stars, 332 42

Hamann, W.-R., Koesterke, L., & Wessolowski, U. 1995, Astronomy and Astrophysics, 299, 151 17, 42

Heger, A., Langer, N., & Woosley, S. E. 2000, The Astrophysical Journal, 528, 368 8, 10

Heger, A. & Woosley, S. E. 2002, The Astrophysical Journal, 567, 532 8

Humphreys, R. M. & Davidson, K. 1979, The Astrophysical Journal, 232, 409 v, 13

Humphreys, R. M. & Davidson, K. 1994, Publications of the Astronomical Society of the Pacific, 106, 1025 v, 8, 21

Hunter, I., Lennon, D. J., Dufton, P. L., et al. 2008, Astronomy and Astrophysics, 479, 541 9, 10, 29

Iglesias, C. A. & Rogers, F. J. 1996, The Astrophysical Journal, 464, 943 20

Iglesias, C. A., Rogers, F. J., & Wilson, B. G. 1992, The Astrophysical Journal, 397, 717 3

Kippenhahn, R. & Thomas, H.-C. 1970, in Stellar Rotation 9

Kippenhahn, R. & Weigert, A. 1994, Stellar Structure and Evolution (Astronomy and Astrophysics Library), 3rd edn. (Springer), 468 1

Köhler, K. & Langer, N. 2012, 1 14, 15, 25, 43

Kosovichev, A. G. 2007, Proceedings of the International Astronomical Union, 2, 113 9

Kupka, F. 2005, Proceedings of the International Astronomical Union, 2004 9

Kupka, F. & Montgomery, M. H. 2002, Monthly Notices of the Royal Astronomical Society, 330, L6 9

Lamers, H. & Leitherer, C. 1993, The Astrophysical Journal, 412, 771 8

Langer, N. 1991, Astronomy and Astrophysics, 252, 669 9, 10

Langer, N. 1997, in Astronomical Society of the Pacific Conference Series, Vol. 120, Luminous Blue Variables: Massive Stars in Transition, ed. A. Nota & H. Lamers, 83 4, 10, 14

Langer, N. 1998, Astronomy and Astrophysics 15, 43

Langer, N. 2012, Annual Review of Astronomy and Astrophysics, 50 v, 12, 15, 16, 43

Langer, N., Fricke, K. J., & Sugimoto, D. 1983, Astronomy and Astrophysics, 126 10

Low, B. C. 1996, Solar Physics, 167, 217 7

Lucy, L. B. & Solomon, P. M. 1970, The Astrophysical Journal, 159, 879 11

Mackey, J., Mohamed, S., Neilson, H. R., Langer, N., & Meyer, D. M.-A. 2012, The Astrophysical Journal, 751, L10 8

Maeder, A. & Meynet, G. 2000, Astronomy and Astrophysics 8, 15, 43

Maeder, A. & Meynet, G. 2010, New Astronomy Reviews, 54, 32 8, 15

Moffat, A. F. J. 2008, in Clumping in Hot-Star Winds, 17 12

Mokiem, M. R., de Koter, A., Evans, C. J., et al. 2007a, Astronomy and Astrophysics, 465, 1003 17

Mokiem, M. R., de Koter, A., Evans, C. J., et al. 2007b, Astronomy and Astrophysics, 465, 1003 42

Morton, D. C. 1967, The Astrophysical Journal, 147, 1017 11

Muijres, L. E., de Koter, A., Vink, J. S., et al. 2010, Astronomy & Astrophysics, 526, A32 12

Nieuwenhuijzen, H. & de Jager, C. 1990, Astronomy and Astrophysics, 231, 134 17, 25, 42

Papaloizou, J. C. B., Alberts, F., Pringle, J. E., & Savonije, G. J. 1997, Monthly Notices of the Royal Astronomical Society, 284, 821 14

Parkin, E. R., Pittard, J. M., Corcoran, M. F., Hamaguchi, K., & Stevens, I. R. 2009, Monthly Notices of the Royal Astronomical Society, 394, 1758 8

Peimbert, M., Luridiana, V., & Peimbert, A. 2007, The Astrophysical Journal, 666, 636 20

Petrovic, J., Langer, N., Yoon, S.-C., & Heger, A. 2005, Astronomy and Astrophysics, 435, 247 8

Pistinner, S. & Eichler, D. 1995, The Astrophysical Journal, 454, 404 42

Prialnik, D. 2000, An Introduction to the Theory of Stellar Structure and Evolution (Cambridge University Press), 276 v, 2, 5

Sana, H. & Evans, C. J. 2011, Proceedings of the International Astronomical Union, 6, 474 43

Schaerer, D., de Koter, A., Schmutz, W., & Maeder, A. 1996, Astronomy and Astrophysics 43

Shaviv, N. J. 2001, The Astrophysical Journal, 549, 1093 14

Spiegel, E. A. & Zahn, J.-P. 1977, Lecture Notes in Physics, Vol. 71, Problems of Stellar Convection, ed. E. A. Spiegel & J.-P. Zahn (Berlin, Heidelberg: Springer Berlin Heidelberg) 14

Spruit, H. C. 2002, Astronomy and Astrophysics, 381, 923 10

Vink, J. S., de Koter, A., Lamers, H. J. G. L. M., et al. 2000, Astronomy & Astrophysics, 309, 295 15, 17, 18, 41, 42, 43

Vink, J. S., Koter, A. D., Lamers, H. J. G. L. M., & de Koter, A. 2001, Astronomy & Astrophysics, 369, 574 12, 17

Vink, J. S., Muijres, L. E., Anthonisse, B., et al. 2011, Astronomy & Astrophysics, 531, A132 v, 8, 13, 14, 15, 18, 38, 42, 43

Walborn, N. R., Ebbets, D. C., Parker, J. W., Nichols-Bohlin, J., & White, R. L. 1992, The Astrophysical Journal, 393, L13 v, 12

Yoon, S.-C., Langer, N., & Norman, C. 2006, Astronomy and Astrophysics, 460, 199 8, 17

Yusof, N., Abu Kassima, H., Hirschi, R., et al. 2010, arXiv 17

Zahn, J.-P., Brun, A. S., & Mathis, S. 2007, Astronomy and Astrophysics, 474, 145 10

Appendix A

Extra graphs

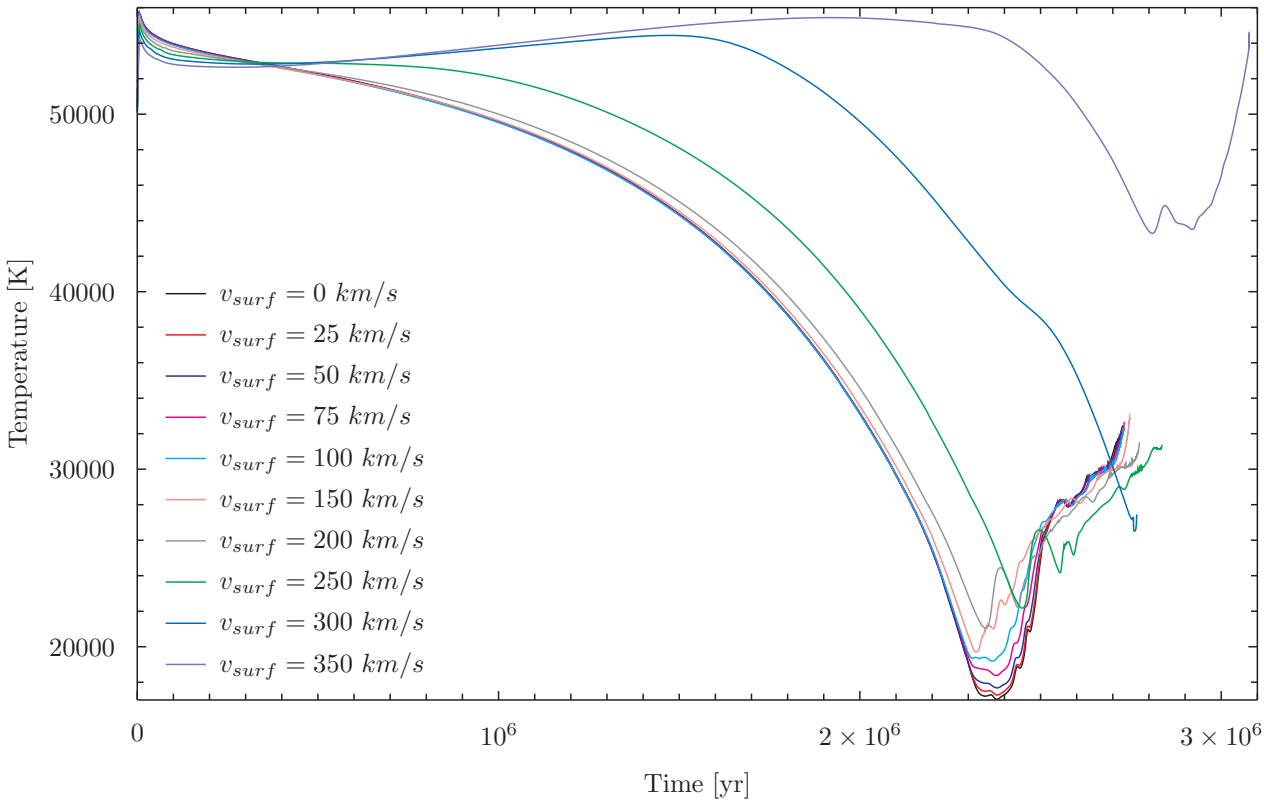

Fig. A.1: The effective temperature as a function of time for $100 M_{\odot}$ models.

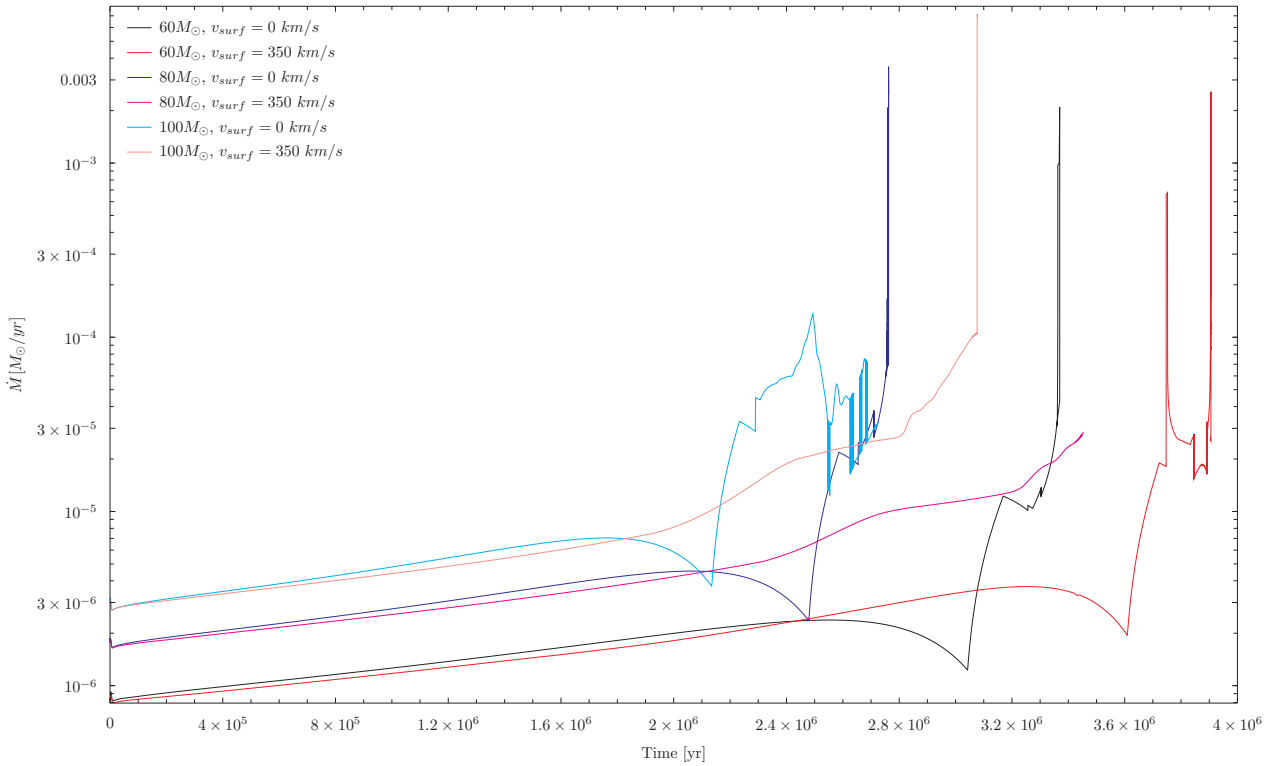

Fig. A.2: The mass loss rates of a selection of models using the $\tau_{max} = 30$ and $b = 1$.